



DIPLOMARBEIT

Visualization and Sonification in QCD and QED

AUSGEFÜHRT AM

ATOMINSTITUT DER ÖSTERREICHISCHEN UNIVERSITÄTEN
DER TECHNISCHEN UNIVERSITÄT WIEN

UNTER DER ANLEITUNG VON

AO.UNIV.PROF. DIPL.-ING. DR.TECHN. HARALD MARKUM

DURCH

ING. NATASCHA HÖRMANN
Matrikelnummer: 9026090
Pillergasse 12/6/9, A-1150 Wien

WIEN, MAI 2006

Contents

1	Introduction	1
1.1	Visualization and Sonification	1
1.2	Sonification Package	3
1.3	Applications of Sonification	3
1.4	Applications in this Thesis	5
2	Theory of QCD and QED	6
2.1	Lattice Quantum Chromodynamics	6
2.1.1	QCD Lagrangian	6
2.1.2	Path Integral and Statistical Mechanics	7
2.1.3	Lattice Regularization	10
2.1.4	Discretized Gluonic Action	11
2.1.5	Fermions on the Lattice	13
2.1.6	Monopoles and Confinement	18
2.1.7	Finite Temperature on the Lattice	19
2.1.8	Numerical Simulation	20
2.2	Lyapunov Exponent in U(1) and SU(2) Gauge Theory	23
2.2.1	Classical Chaotic Dynamics	23
2.2.2	Initial States Prepared by Quantum Monte Carlo	24

3	Sonification Results	26
3.1	Dirac Operator for Fixed Beta	26
3.2	Dirac Operator as a Function of Beta	30
3.3	Disorder Parameter for Magnetic Monopoles	33
3.4	Lyapunov Exponent in U(1) and SU(2) Theory	35
3.5	Physical Observables across Phase Transitions in Polymers	44
4	Summary and Conclusion	46
A	SuperCollider Functions	48
A.1	Short Introduction into the Function Syntax	48
A.2	Functions Used in the Lyapunov Program	49
A.2.1	Impulse – Impulse Oscillator	49
A.2.2	Decay2 – Exponential Decay	49
A.2.3	Osc – Interpolating Wavetable Oscillator	50
A.2.4	AmpComp – Basic Psychoacoustic Amplitude Compensation	51
A.2.5	Splay	52
B	Lyapunov Program	53
B.1	Sonification Program Lyapunov.sc	53
B.2	Input File lyapunov_input_u1.txt	57
B.3	Input File lyapunov_input_su2.txt	58
	Bibliography	60

List of Figures

1.1	Sonification Process	2
3.1	Configuration-averaged values of the 15 lowest levels of the eigenvalue spectrum of the Dirac operator for 6 different couplings β	27
3.2	Eigenvalue spectra transformed into audible region for β -values across the phase transition from quark confinement to the quark-gluon plasma.	28
3.3	Screenshots of the low-lying part of the spectrum of the Dirac operator in the confinement and deconfinement region.	29
3.4	Configuration-averaged values of the 15 lowest levels of the eigenvalue spectrum of the Dirac operator as a function of the gluon coupling β	30
3.5	Six selected eigenvalues transformed into the audible region for values of β across the QCD phase transition.	31
3.6	Screenshots of the lowest and the 10^{th} eigenvalue of the Dirac operator moving from the confinement to the deconfinement region.	32
3.7	Monopole disorder parameter ρ computed by the Pisa group as a function of β for different spatial sizes at fixed $N_t = 4$ with Polyakov projection and Abelian generator F^3	33
3.8	Snapshots of the zero-value at small couplings and of the spike of the monopole disorder parameter at the transition point.	34
3.9	Exponentially diverging distance of initially adjacent $U(1)$ field configurations on a 12^3 lattice prepared at $\beta = 0.9$ in the confinement phase (top) and at $\beta = 1.1$ in the Coulomb phase (bottom).	36
3.10	Transition of the leading Lyapunov exponents from 100 $U(1)$ configurations as a function of the inverse coupling strength β	37

3.11	Transition of the plaquette energy as in Fig. 3.10.	37
3.12	Scatter plots of Lyapunov exponents and plaquette energies for 100 $U(1)$ configurations.	38
3.13	Comparison of the average maximal Lyapunov exponent in $U(1)$ gauge theory with $\beta = 1/g^2$ (top) and in $SU(2)$ gauge theory with $\beta = 4/g^2$ (bottom) when crossing from the strong to the weak coupling phase.	39
3.14	Comparison of the average plaquette energy as in Fig. 3.13 . . .	40
3.15	Comparison of average maximal Lyapunov exponents as a function of the scaled average energy per plaquette ag^2E . The $U(1)$ theory (top) shows an approximately quadratic behavior in the weak coupling regime whereas the $SU(2)$ theory (bottom) is approximately linear.	41
3.16	Comparison of the audible frequencies of the Lyapunov exponent in $U(1)$ gauge theory (top) and in $SU(2)$ gauge theory (bottom) when crossing from the strong to the weak coupling phase.	43
3.17	Solubility-temperature pseudophase diagram of a 179-mer simulated by the Leipzig group. The color codes the specific heat as a function of reciprocal solubility s and temperature T	45
3.18	Expectation values, self- and cross-correlations of the contact numbers n_s and n_m as functions of the temperature T in comparison with the specific heat C_V for a 179-mer in solvent with $s = 1$. The specific heat from these results of the Leipzig group is taken for sonification.	45

Kurzfassung

Sonifikation wird zur Verklanglichung von Informationen aus Daten verwendet und ist das Analogon zur grafischen Darstellung. Die Methode wird in zahlreichen Disziplinen wie Ökonomie, Medizin oder Physik angewendet. Wir untersuchten, ob eine derartige Analyse auch für den Phasenübergang der Quantenchromodynamik vorteilhaft ist, um das Verhalten von physikalischen Observablen als Funktion von Parametern wie Temperatur, Eichkopplung, Quarkmasse und anderen Variablen des Systems zu bestimmen. Weiters versuchten wir herauszufinden, ob es möglich ist versteckte Eigenschaften zu entdecken, welche in der graphischen Darstellung nicht erkennbar sind.

Um die Methodik der Sonifikation für die Quantenchromodynamik zu veranschaulichen, analysierten wir die Eigenwerte des Dirac-Operators von der Confinement zur Deconfinement-Phase. Wir verarbeiteten das Spektrum für aufsteigende Eigenwerte mit fester Gluonkopplung β und in einer zweiten Auswertung fixierten wir die Eigenwerte als Funktion von β . Als nächstes erzeugten wir ein Sound-File aus den Daten des Disorder-Parameters für magnetische Monopole. In einem weiteren Beispiel analysierten wir den Lyapunov-Exponenten für klassische $U(1)$ und $SU(2)$ Eichfeldkonfigurationen auf einem Gitter, welche durch Quanten-Monte-Carlo-Simulation erzeugt wurden. Zum Abschluß sonifizierten wir die spezifische Wärme von Polymeren, die eine komplexe Phasenstruktur besitzen.

Zur Erstellung der Audio-Files reskalierten wir die Rohdaten in den hörbaren Frequenz-Bereich mit dem Kammerton von 440 Hz als Referenz. Wir variierten die Klang-Attribute wie Dauer, Anstieg-/Abklinggeschwindigkeit, Klangfarbe und räumliche Position, um die Charakteristik der Daten herauszuhören. Dann generierten wir ein Audio-File und wandelten es in ein mp3-File um. Diese Files können am SonEnvir Server www.sonenvir.at aufgerufen werden.

Die vorliegenden ersten Versuche von Sonifikation in der Gitterfeldtheorie zeigen, dass die erkennbaren Strukturen im Sound-File ähnlich jenen in der grafischen Darstellung sind. In dieser Hinsicht kann Sonifikation, wie hier angewendet, als zusätzliches Werkzeug zur Präsentation von Daten angesehen werden. Datenanalyse durch Sonifikation könnte sinnvoll sein für die Darstellung von Ergebnissen, welche von mehreren Parametern und/oder höheren Raum-Zeit-Dimensionen abhängen. Das Sonifikations-Programm wurde in Zusammenarbeit mit der Universität für Musik und Darstellende Kunst in Graz und der Universität von Graz entwickelt, wo das interdisziplinäre Forschungsprojekt SonEnvir durchgeführt wird.

Abstract

Sonification is the use of non-speech audio to extract information from data and represents the sound analogue to graphical visualization. The method is applied in several disciplines as economy, medicine or physics. We investigated if it might help to analyze lattice data and critical phenomena, together with graphical display, in order to examine the behavior of physical observables as a function of parameters like temperature, gauge coupling, quark mass and other variables of the system. Furthermore, we wanted to find out, if it is possible to discover hidden features which cannot be seen in graphical diagrams.

To demonstrate the methodology of sonification for quantum chromodynamics we analyzed the eigenvalues of the Dirac operator from the confinement to the deconfinement phase. We used the spectra for ascending eigenvalues keeping β fixed and in a second sample we fixed the eigenvalues as a function of the coupling β . Next we produced a sound file for the data of the disorder parameter for magnetic monopoles. In a further example we analyzed the leading Lyapunov exponents of classical $U(1)$ and $SU(2)$ gauge field configurations on the lattice which were initialized by quantum Monte Carlo simulations. In a last step we sonified the specific heat belonging to the rich energy landscape of certain polymers.

For the preparation of the audio files we rescaled the raw data into an audible frequency range with the standard pitch of 440 Hz as reference. We varied the sound attributes like duration, attack/decay rate, timbre and location of the sound to extract characteristics of the data. Then we generated audio files and transformed them to mp3-files. They can be accessed from the SonEnvir Server at www.sonenvir.at.

In the underlying first trials of sonification in lattice field theory, the structures one could recognize from the sound files are similar to those from graphical visualization. In this regard, sonification as applied here can be seen as an additional tool of data representation. Data analysis through sonification might especially be useful for displaying results depending on multiple parameters and/or belonging to higher space-time dimensions. The sonification program was developed together with the University of Music and Dramatic Arts in Graz and the University of Graz where the interdisciplinary research project SonEnvir is based.

1

Introduction

1.1 Visualization and Sonification

Data presentation techniques in general are based on data visualization. However, there is an alternative which might be superior for certain types of data: acoustic data presentation, called *sonification*. This new research area could help to analyze complex, high-dimensional or a huge amount of data with new techniques. While visualization addresses the visual sense, sonification addresses the sense of listening, a perceptual channel which is so far rather neglected for the analysis of data. However, besides supporting the analysis of data structures themselves, sonification finds application in various other fields, e.g. to replace visual perception for blind people or to support navigation in virtual environments, or to assist the monitoring of complex processes.

In modern science and economy a vast amount of relevant data is stored and made available for evaluation. Techniques to locate the numbers of interest like data warehousing and data mining have been developed together with program packages for visualization in order to extract the information hidden. The question arose if methods of auditory display could help to get further insight into the structures behind the data.

The sonification process consists of several parts. The central element is the sonification model which assesses the interesting data as input and produces a sound file as output. The user interacts with the sonification model, adapting

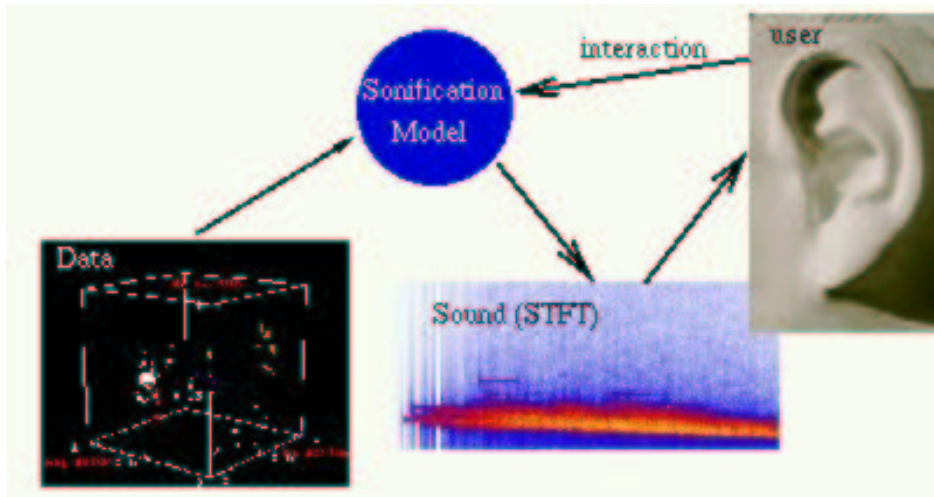


Figure 1.1 Sonification Process

its structure and fitting the model parameters iteratively in order to uncover the information (Fig. 1.1 [1]).

Sonification can make use of several sound attributes for presenting various data characteristics. We list the most important attributes [2]

- pitch – perceived frequency of a sound
- loudness – the magnitude of a sound
- duration – the length of time a sound is heard
- timbre – the general prevailing quality or characteristic of a sound
- attack/decay rate – the time it takes a sound to reach its maximum/minimum
- spatial hearing – location of a sound

The International Community for Auditory Display (ICAD) covers many activities in the field of sonification [3]. The ICAD was established in 1992 and has been organizing international conferences since then. At the request of the NSF in 1997 the ICAD provided a Sonification Report [4].

1.2 Sonification Package

Sonification needs a realization on software and hardware platforms. A widely used program package for sonification is called SuperCollider and was developed by James McCartney from Austin, TX. It started as proprietary software and was released in 2002 under the open software GPL license. The name SuperCollider is said to have its origin from the Superconducting Super Collider (SSC) in Waxahachie, TX, which was planned and begun to be constructed but was then abandoned and never finished.

SuperCollider is an environment and programming language for real time audio synthesis. The programs to generate or process sound can be executed in real time or not. They can be controlled by MIDI (Musical Instrument Digital Interface), the mouse, graphics tablets, and over a network via Open Sound Control. The environment consists of two applications, a client *sclang* (the language part) and a server *scsynth* (the audio part) which communicate using Open Sound Control. The language (*sclang*) is an interpreter language and combines the object oriented structure of Smalltalk and features from functional programming languages with a C programming language family syntax. SuperCollider is a free program and runs on MacOS, Linux and Windows [5].

Beside this professional solution general mathematical analysis programs, such as Matlab, Mathematica, or Maple, are sometimes used to do research on sound signal processing and synthesis algorithms. But most commercially available signal analysis packages do not support real-time signal processing and direct control of sound input or output [4].

1.3 Applications of Sonification

Sonification is used in different fields for analyzing complex or high-dimensional data [6]

- physics
- psychology
- physiology
- mathematics and computer science
- sound engineering
- algorithmic composition / sound art

- epistemology and sociology of science

In the following an overview of the research areas of the SonEnvir project is given. SonEnvir is an interdisciplinary project that investigates sonification in a number of scientific disciplines, in order to develop a general sonification software environment. It is a collaboration of four universities in Graz, Austria: The Karl Franzens University, the University of Technology, the Medical University, and the University for Music and Dramatic Arts [5].

Electronic Music and Acoustics The Institute of Electronic Music and Acoustic (IEM) is the host institution and the basis for sound expertise in SonEnvir. The goal is to apply the technologies developed at the IEM to the problems in sonification and push the field scientifically as well as aesthetically.

Neurology In neurology, sonification is utilized to analyze EEG-data. The EEG (electroencephalogram) is a diagnostic method used for patients with epilepsy, cerebral function disorders, tumors and insults. Characteristics of this method is good resolution of data concerning time, but bad resolution concerning space. Sonification can ease the daily routine of monitoring by sending acoustic signals which alert the staff to react quickly on atypical brain events (epileptic fit). Moreover, it is possible to gain information about epileptic mechanisms in general and how an epileptic fit can be detected before its occurrence. Sonification of EEG-data is a further step to multi-media diagnostics in epilepsy.

Sociology Up to now sonification only was applied in fields of natural science. It offers a method complementary to the usual data exploration techniques that can also be used within social scientific contexts. Many research branches in the social sciences are concerned with events or actions in a temporal context. Due to its inherent time factor, sonification can be a valuable technique for the exploration of sequential data sets.

Theoretical Physics Elementary particle physics is interested in the study of baryons being composed of three quarks. Within a relativistic constituent-quark model the mass spectra with different types of interactions between the quarks, the baryon ground states and the decay widths of the baryon resonances have been investigated. In theoretical physics it is common to use graphical methods for data analysis. Audible data analysis was so far basically unknown and the first method of sonification was in respect to the evaluation of baryon properties. The resulting approach should serve as a prototype for investigating more complicated data sets.

Concerning the analysis of the baryon spectra via sonification the question arose if it is possible to discover hidden symmetries (or symmetry breaking) which cannot be seen in graphical diagrams [7].

Signal Processing and Speech Communication Problem domains investigated in SonEnvir include electro-magnetic wave propagation (multi-path propagation) in mobile applications and signal classification problems (e.g. non-deterministic chaos).

1.4 Applications in this Thesis

This diploma thesis was inspired and partly supported by the SonEnvir project [5]. The main goal was the application of auditory display to data from physical observables across phase transitions. The studies range from quantum chromodynamics to polymers. Central emphasis will be on the phase transition of QCD from the confinement of quarks to the plasma of quarks and gluons. The physical observable is the eigenvalue spectrum of the Dirac operator of a quark in QCD. In two analyses of the lowest eigenvalues, keeping the gluonic coupling β fixed and letting β run, respectively, we will sonify the restoration of chiral symmetry when increasing the coupling to the quark-gluon plasma-phase. Subsequently, the disorder parameter for magnetic monopoles will be considered. We shall listen to the spike at the phase transition to the quark-gluon plasma where the monopoles vanish.

The next study will be devoted to the leading Lyapunov exponents of $U(1)$ and $SU(2)$ classical gauge field configurations on the lattice. It will be interesting to hear the breakdown of the Lyapunov exponent at the phase transition, and to probe the difference between the first and second order of both transitions.

The last analysis will deal with Monte Carlo simulations of polymers which exhibit a rich phase structure. Sonification of the landscape of the specific heat with spikes, valleys and saddle points will be challenging.

Theory of QCD and QED

2.1 Lattice Quantum Chromodynamics

2.1.1 QCD Lagrangian

Today, Quantum Chromodynamics (QCD) is believed to be the fundamental theory of strong interactions [8, 9]. It was constructed along the lines of the very successful Quantum Electrodynamics (QED) as a quantized gauge field theory with a local gauge symmetry. For this reason the Lagrangian of QCD looks similar to that of QED. In contrast to the Abelian $U(1)_{\text{elm}}$ gauge symmetry of QED, the field equations of QCD are invariant under non-Abelian $SU(3)_{\text{color}}$ gauge transformations. Whereas in QED electrons and photons are the fundamental particles, in QCD quarks and gluons are the basic degrees of freedom. Quarks are fermionic matter fields. They transform according to the fundamental triplet representations of $SU(3)_{\text{color}}$. Gluons are bosonic gauge fields and transform according to the octet representation. So the Lagrangian consists of a gluonic and a fermionic part,

$$\begin{aligned} \mathcal{L}^{\text{QCD}} &= \mathcal{L}_{\text{G}}^{\text{QCD}} + \mathcal{L}_{\text{F}}^{\text{QCD}} \\ &= -\frac{1}{4}F_{\mu\nu}^a(x)F_a^{\mu\nu}(x) + \sum_{f=1}^{n_f} \bar{\psi}_f(x)(iD - m_f)\psi_f(x); \end{aligned} \quad (2.1)$$

ψ_f is the Dirac spinor, m_f the quark mass and n_f the number of flavors. The generalized field strength tensor $F_a^{\mu\nu}(x)$ is

$$F_a^{\mu\nu}(x) = \partial^\mu A_a^\nu(x) - \partial^\nu A_a^\mu(x) - gf_{abc}A_b^\mu(x)A_c^\nu(x), \quad (2.2)$$

where $a, b, c = 1, \dots, 8$ are $SU(3)$ indices. A_a^μ is the gauge field, g the coupling constant, and f_{abc} are the structure constants of $SU(3)$. The gauge covariant derivative

$$D^\mu(x) = \partial^\mu + igA_a^\mu(x)\frac{\lambda^a}{2}, \quad (2.3)$$

with the generators λ_a of $SU(3)$ (Gell-Mann matrices), induces the minimal gauge invariant interaction with strength g [10].

The Lagrangian (2.1) enables the formulation of QCD as a quantum field theory. One possible quantization is the path integral formulation of QCD. Renormalizability and asymptotic freedom can be proven and there are several theoretical hints for quark confinement. Because of these features QCD is believed to be the right theory of hadron physics.

2.1.2 Path Integral and Statistical Mechanics

The path integral formalism [11] is a very powerful method for calculating observables in QCD [8]. To explain the path integral we first consider a particle in quantum mechanics. In contrast to classical mechanics, where the exact “path” of a particle is known, in quantum mechanics one has to calculate transition amplitudes

$$\langle q'_t | q_{t_0} \rangle, \quad (2.4)$$

where $|q_{t_0}\rangle$ and $|q'_t\rangle$ are eigenstates of the space coordinate operator $Q(t)$ in the Heisenberg picture. The absolute square of the transition amplitude (2.4) is proportional to the probability that a particle which at the time t_0 was located at q , at the time t will be found at the place q' .

There exist infinitely many paths connecting the initial with the final point. Dividing the time interval $[t_0, t]$ into $N + 1$ equidistant time steps δt and inserting complete systems $\int dq_{t_i} |q_{t_i}\rangle \langle q_{t_i}|$ in (2.4) one obtains

$$\langle q'_t | q_{t_0} \rangle = \int dq_{t_1} \dots dq_{t_N} \langle q'_t | q_{t_N} \rangle \dots \langle q_{t_2} | q_{t_1} \rangle \langle q_{t_1} | q_{t_0} \rangle. \quad (2.5)$$

For infinitesimal time intervals it is sufficient to consider a path that fulfills

$$\langle q_{t+\delta t} | q_t \rangle \propto e^{iS(q_t, q_{t+\delta t})}, \quad (2.6)$$

with the action

$$S = \int dt L \quad (2.7)$$

obtained from the Lagrangian L . From (2.5) and (2.6) it follows that

$$\langle q'_t | q_{t_0} \rangle \propto \lim_{N \rightarrow \infty} \int \prod_{i=1}^N dq_{t_i} e^{iS[q(t)]} =: \int \mathcal{D}[q] e^{iS[q(t)]} . \quad (2.8)$$

So to calculate a quantum mechanical transition amplitude one has to integrate over all possible paths, weighted with the phase factor $\exp(iS[q(t)])$. In classical mechanics only the path with minimal action is taken into account.

Within the path integral formalism of QCD a quantum field theoretical vacuum expectation value of an operator is calculated according to

$$\langle O \rangle = \langle 0 | O | 0 \rangle = \frac{1}{Z} \int \mathcal{D}[A] \mathcal{D}[\psi] \mathcal{D}[\bar{\psi}] e^{iS[A, \psi, \bar{\psi}]} O(A, \psi, \bar{\psi}) , \quad (2.9)$$

with the vacuum-to-vacuum transition amplitude

$$\langle 0 | 0 \rangle = \int \mathcal{D}[A] \mathcal{D}[\psi] \mathcal{D}[\bar{\psi}] e^{iS[A, \psi, \bar{\psi}]} =: Z . \quad (2.10)$$

In QCD the functional integration extends over all gauge field configurations $A_a^\mu(x)$ (Lorentz index $\mu = 0, \dots, 3$, group index $a = 1, \dots, 8$) and over all configurations of the fermionic fields $\psi_c^\alpha(x)$ and $\bar{\psi}_c^\alpha(x)$ (spinor index $\alpha = 1, \dots, 4$, color index $c = 1, 2, 3$). Because of the anticommutation relations of the fermionic fields these are represented by Grassmann variables.

The expectation value (2.9) diverges in general for continuous space-time. This is a consequence of the integration over physically equivalent gauge field configurations due to the gauge freedom. To avoid this divergence one has to fix the gauge with an additional term \mathcal{L}^{fix} in the Lagrange density \mathcal{L}^{QCD} . This constrains the system and therefore the integration is done over a restricted range of parameters. In terms of the old integration variables the emerging functional determinant can be interpreted as a path integral over new Grassmann fields, the so-called Fadeev-Popov ghosts, leading to the Lagrangian $\mathcal{L}^{\text{ghost}}$. Thus, the complete Lagrange density of QCD is

$$\mathcal{L} = \mathcal{L}^{\text{QCD}} + \mathcal{L}^{\text{fix}} + \mathcal{L}^{\text{ghost}} . \quad (2.11)$$

Except for the explicit calculation of gluon or quark propagators, gauge fixing is not needed for gauge invariant objects in the lattice formulation of QCD, since a finite number of integrations is performed with the finite Haar measure. Further

problems of the path integral formalism like a mathematically sound definition of the integration measure $\mathcal{D}[A, \psi, \bar{\psi}]$ or oscillations due to the imaginary weight factor $e^{iS[A, \psi, \bar{\psi}]}$ do not occur on a Euclidean space-time lattice.

Despite of the imaginary exponent the vacuum expectation value (2.9) is reminiscent of a thermodynamical average in statistical mechanics. For a complete analogy between statistical mechanics and the path integral formulation of QCD one has to change from Minkowski to four-dimensional Euclidean space. This is achieved by an analytical continuation to imaginary time

$$t =: x_0 \rightarrow -ix_4 \quad \text{with real } x_4. \quad (2.12)$$

With $\partial_0 = i\partial_4$, $p_0 = ip_4$, and $A_0 = iA_4$ one obtains after a short calculation the relation between the gluonic Lagrangians \mathcal{L}_G^M and \mathcal{L}_G^E in Minkowski and Euclidean space ($i, j = 1, 2, 3$)

$$\begin{aligned} \mathcal{L}_G^M &= -\frac{1}{4}F_{\alpha\beta}^a(x)F_{\alpha\beta}^a(x) = -\frac{1}{4}\left(F_{ij}^a(x)F_{ij}^a(x) - 2F_{0j}^a(x)F_{0j}^a(x) + F_{00}^a(x)F_{00}^a(x)\right) \\ &= -\frac{1}{4}\left(F_{ij}^a(x)F_{ij}^a(x) + 2F_{4j}^a(x)F_{4j}^a(x) + F_{44}^a(x)F_{44}^a(x)\right) = -\frac{1}{4}F_{\mu\nu}^a(x)F_{\mu\nu}^a(x) \\ &=: -\mathcal{L}_G^E. \end{aligned} \quad (2.13)$$

Here, $\alpha, \beta = 0, \dots, 3$ are four indices in Minkowski space, and $\mu, \nu = 1, \dots, 4$ are those in Euclidean space. For the fermionic Lagrangian one obtains

$$\mathcal{L}_F^M = \bar{\psi}(x)(iD - m)\psi(x) = -\bar{\psi}(x)(D_\mu\gamma_\mu + m)\psi(x) =: -\mathcal{L}_F^E. \quad (2.14)$$

The Euclidean γ matrices fulfill the anticommutation relations

$$\{\gamma_\mu, \gamma_\nu\} = 2\delta_{\mu\nu}. \quad (2.15)$$

A possible choice for the γ matrices is

$$\gamma_4 = \begin{pmatrix} 1 & 0 \\ 0 & -1 \end{pmatrix}, \quad \gamma_i = \begin{pmatrix} 0 & \sigma_i \\ \sigma_i & 0 \end{pmatrix}, \quad (2.16)$$

with the Pauli matrices σ_i . They are Hermitian

$$\gamma_\mu = \gamma_\mu^\dagger. \quad (2.17)$$

With $i \int dx_0 = \int dx_4$ one obtains the complete Euclidean action

$$\begin{aligned} iS^M &= i \int d^4x (\mathcal{L}_G^M + \mathcal{L}_F^M) = i \int dx_0 d^3x (\mathcal{L}_G^M + \mathcal{L}_F^M) = \\ &= \int dx_4 d^3x (-\mathcal{L}_G^E - \mathcal{L}_F^E) =: -S^E. \end{aligned} \quad (2.18)$$

The vacuum expectation value of an observable in the Euclidean path integral formulation is

$$\langle O \rangle = \frac{1}{Z} \int \mathcal{D}[A] \mathcal{D}[\psi] \mathcal{D}[\bar{\psi}] e^{-S^E[A, \psi, \bar{\psi}]} O(A, \psi, \bar{\psi}), \quad (2.19)$$

with

$$Z = \int \mathcal{D}[A] \mathcal{D}[\psi] \mathcal{D}[\bar{\psi}] e^{-S^E[A, \psi, \bar{\psi}]}. \quad (2.20)$$

By imposing periodic boundary conditions in Euclidean time a total analogy with statistical mechanics is achieved, and Z can be viewed as a partition function of a thermodynamical system. For many physical problems like the calculation of the mass of a particle from the asymptotic behavior of its propagator one can obtain results directly from the Euclidean formulation. Therefore, a return to Minkowski space often is not necessary.

2.1.3 Lattice Regularization

A well-defined expression for the path integral of a quantum mechanical particle can be obtained by discretizing the time variable [8]. Since a continuous path $x(t)$ now turns into a sequence of points $x_k = x(t_k)$ ($k = 0, 1, \dots, n+1$), the functional integration over all paths $x(t)$ simplifies to an ordinary integration over the variables x_k ($k = 1, 2, \dots, n$). Performing the limit $n \rightarrow \infty$ at the end of the calculation one returns to continuum time.

In a field theory the dynamical variables are the local fields and depend on the four Euclidean space-time variables. A generalization of the above procedure leads to the construction of a four-dimensional hypercubic lattice with the lattice spacing a and the lattice points $x = (x_1, x_2, x_3, x_4)$, where x_1, \dots, x_4 are integers. Defining the fields on this Euclidean space-time lattice one obtains a discrete set of variables. The functional integration over all field configurations simplifies to an integration over these variables.

The Fourier transform of a function $f(x)$ defined on the periodic lattice

$$\tilde{f}(p) = a^4 \sum_x e^{ipx} f(x) \quad (2.21)$$

is periodic in p with the period $p_\mu = \frac{2\pi}{a}$. Therefore momentum is restricted to the first Brillouin zone $-\frac{\pi}{a} < p_\mu \leq \frac{\pi}{a}$. This removes ultraviolet divergencies. So the introduction of a lattice provides a regularization scheme.

Internal symmetries survive discretization whereas spatial symmetries are broken. This is obvious for the Euclidean Poincaré group, which contains $O(4)$ rotations, but on the lattice only rotations through multiples of $\frac{\pi}{2}$ are allowed. The

big advantage is that local gauge invariance can be preserved. Furthermore, in the limit $a \rightarrow 0$ one should recover the continuum theory. However, there is no unique choice of a discrete action fulfilling this requirement.

Scalar and vector fields are located on the sites and links of the lattice, respectively. The association of spinors to the lattice is much more involved. The discretization of fermionic degrees of freedom is a difficult problem of lattice gauge theory.

2.1.4 Discretized Gluonic Action

As a first step one defines gluonic fields on the lattice [8]. A naive discretization of the continuum equations by simply assigning the vector potentials to the links and substituting all derivatives with finite differential quotients would violate local gauge invariance for finite lattice spacing a . The covariant derivative has the correct transformation behavior only in the continuum limit $a \rightarrow 0$.

The differential geometry of local gauge fields opens up a possibility for their definition on the lattice [10]. The gauge transformation

$$\phi(x) \rightarrow \exp\left(ig\theta_a(x)\frac{\lambda_a}{2}\right)\phi(x) = g(x)\phi(x) \quad (2.22)$$

can be understood as a coordinate transformation when changing the basis of a local charge space ${}^x\mathcal{H}$ at the site x . A comparison of vector fields located at different places x is only possible when their components refer to the same coordinate system. This is achieved via a translation

$${}^x\phi(x) \rightarrow {}^{x+dx}\phi(x) = \left(1 - igA_\mu^a(x)\frac{\lambda_a}{2}dx^\mu\right) {}^x\phi(x), \quad (2.23)$$

where the upper left index indicates the local coordinate system. This transformation preserves the features of the vectors related to unitary symmetry, being linearity, orthogonality and normalization. Starting from (2.23) one obtains the unitary transformation for finite translations along a curve \mathcal{C}

$$U(\mathcal{C}) = \mathcal{P} \exp\left(ig \int_{\mathcal{C}} dx^\mu A_\mu^a(x)\frac{\lambda_a}{2}\right), \quad (2.24)$$

where \mathcal{P} is a path ordering operator. It guarantees that sectors of \mathcal{C} are not commuted when summing up the exponential series.

We now consider the lattice and define the matter fields $\phi(x)$ on the lattice sites. Then the translations of charged fields are described by gauge fields defined on links

$$U_{x\mu} = \mathcal{P} \exp \left(ig A_{x\mu}^a \frac{\lambda^a}{2} \right). \quad (2.25)$$

So the basic gauge fields on the lattice are the fields $U_{x\mu}$. In QCD they are $SU(3)$ fields describing the parallel transport of a color charge from x to $x + \hat{\mu}$, with the unit vector $\hat{\mu}$ in the direction μ . The transportation of a charge in opposite direction is described by the Hermitian conjugated gauge field

$$U_{x+\hat{\mu},-\mu} = U_{x\mu}^\dagger = U_{x\mu}^{-1}. \quad (2.26)$$

Requiring local gauge invariance for

$$\phi_x^\dagger U_{x\mu} \phi_{x+\hat{\mu}} \quad (2.27)$$

one obtains the transformation law

$$U_{x\mu} \rightarrow g_x U_{x\mu} g_{x+\hat{\mu}}^{-1}, \quad (2.28)$$

with $g_x \in SU(3)$.

With this definition of the gauge fields on the lattice one can write down the lattice version of the gluonic Lagrange density. There is no unique way of constructing the lattice Lagrangian but it has to converge to the continuum Lagrangian for $a \rightarrow 0$.

In pure gauge theory without sources and sinks the flux lines of the gauge fields are closed loops. The smallest loops on the lattice, called plaquettes, are squares with the edge length a . The corresponding flux is

$$U_{\text{pl},\mu\nu}(x) := U_{x\mu} U_{x+\hat{\mu},\nu} U_{x+\hat{\nu},\mu}^\dagger U_{x\nu}^\dagger. \quad (2.29)$$

Repeated application of the Baker-Hausdorff formula to (2.29) yields

$$U_{\text{pl},\mu\nu}(x) = \exp(iga^2 F_{x,\mu\nu}) = 1 + iga^2 F_{x,\mu\nu} + \frac{1}{2!}(iga^2)^2 (F_{x,\mu\nu})^2 + \dots \quad (2.30)$$

The gauge invariant expression [12]

$$S_G = \beta \sum_{\text{pl}} \left(1 - \frac{1}{3} \text{Re Tr } U_{\text{pl}} \right), \quad (2.31)$$

with the inverse coupling constant $\beta = \frac{6}{g^2}$, converges to the continuum action for $a \rightarrow 0$

$$S_G \xrightarrow{a \rightarrow 0} \int d^4x \frac{1}{4} F_{\mu\nu}(x) F_{\mu\nu}(x). \quad (2.32)$$

The Wilson plaquette action (2.31) is one possible choice for the gluonic action on the lattice.

The pure gluonic expectation value of an observable is

$$\langle O \rangle = \frac{1}{Z} \prod_{\text{links}} \int dU_{x\mu} O(U) e^{-S_G}, \quad (2.33)$$

with the partition function

$$Z = \prod_{\text{links}} \int dU_{x\mu} e^{-S_G}. \quad (2.34)$$

The integration measure with the following features

$$\int dU = 1, \quad \int dU f(U) = \int dU f(VU) = \int dU f(UV), \quad V \in SU(3), \quad (2.35)$$

is called Haar's measure. In contrast to a path integral in the continuum, (2.33) and (2.34) comprise only a finite number of integrals over the gauge group. No gauge fixing is needed for gauge invariant observables. A four-dimensional hypercubic lattice with linear dimension N has $4N^4$ links. An integration over the full gauge group $SU(3)$, for example over the eight Euler angles, has to be performed on each link, resulting in $32N^4$ integrals over a compact interval.

One of the great advantages of the lattice formulation of QCD is that methods of statistical mechanics can be used in a field theory. For small inverse coupling constant β the strong coupling approximation is valid. This is an analogy to the high temperature approximation in statistical mechanics. For large β the weak coupling expansion can be used. For intermediate couplings Monte Carlo methods are successful.

2.1.5 Fermions on the Lattice

Species Doubling

The Euclidean free fermionic continuum action is [8]

$$S_F = \int d^4x \bar{\psi}(x) (\partial_\mu \gamma_\mu + m) \psi(x). \quad (2.36)$$

Following the naive discretization scheme by defining the fermionic fields on the lattice points and substituting the differential operator ∂_μ by the symmetric differential quotient

$$\partial_\mu \hat{=} \frac{1}{2a} (\delta_{x+\hat{\mu},x'} - \delta_{x,x'+\hat{\mu}}), \quad (2.37)$$

yields the following discretized action for free fermions [13]

$$S_F = a^4 \left\{ \frac{1}{2a} \sum_{x,\mu} \left[\bar{\psi}_x \gamma_\mu \psi_{x+\hat{\mu}} - \bar{\psi}_{x+\hat{\mu}} \gamma_\mu \psi_x \right] + m \sum_x \bar{\psi}_x \psi_x \right\}. \quad (2.38)$$

One gets the interacting gauge invariant fermionic lattice action by inserting gauge fields U between the ψ fields into the nonlocal terms

$$S_F = a^4 \left\{ \frac{1}{2a} \sum_{x,\mu} \left[\bar{\psi}_x \gamma_\mu U_{x\mu} \psi_{x+\hat{\mu}} - \bar{\psi}_{x+\hat{\mu}} \gamma_\mu U_{x\mu}^\dagger \psi_x \right] + m \sum_x \bar{\psi}_x \psi_x \right\}. \quad (2.39)$$

In equations (2.38) and (2.39) the color, Dirac and flavor indices are omitted. Together with the action (2.31) we now have a gauge invariant lattice regularized version of QCD.

In fact, the above action is not suitable for describing QCD, because it has a hidden degeneracy in the fermionic degrees of freedom. To see this let us consider a massless free fermion as described by (2.36) for $m = 0$. The propagator in momentum space is

$$G(p) = \frac{1}{\frac{1}{a} \sum_\mu \gamma_\mu \sin(p_\mu a)}. \quad (2.40)$$

Besides the physical pole at $p_\mu a = 0$ there are 15 further poles in the first Brillouin zone at

$$p_\mu a = (\pi, 0, 0, 0), (0, \pi, 0, 0), \dots, (\pi, \pi, 0, 0), \dots, (\pi, \pi, \pi, \pi). \quad (2.41)$$

The naively discretized action describes 16 fermions and consequently cannot reproduce the original continuum Lagrange density in the limit $a \rightarrow 0$.

Fermion doubling is a fundamental problem for all lattice actions that preserve the chiral symmetry in the massless continuum limit. It can be shown that it is impossible to construct a chirally invariant lattice action that is free of degeneracy. A chirally symmetric lattice fermion action is at least four-fold degenerate [14, 15]. One has the choice of an action that is not degenerate in the number of fermions but breaks chiral symmetry explicitly for a finite lattice constant. This is achieved with the Wilson method [12]. The second possibility is to preserve chiral invariance at least partly and to accept a partial fermion degeneracy, like in the Kogut-Susskind method [16, 17]. In the last years there was a breakthrough in the construction of chiral fermions. Unfortunately, all solutions are technically and numerically demanding [18, 19].

Kogut-Susskind Fermions

The original idea of this fermionic discretization scheme is to distribute the components of a spinor over a unit cube instead of defining it on a single lattice point [8]. Now, two corresponding components of the spinor are separated at least by two fundamental lattice spacings. As a consequence the first Brillouin zone reduces to $-\frac{\pi}{2a} < p_\mu \leq \frac{\pi}{2a}$ so that the pole at $\frac{\pi}{a}$ is outside. The degeneracy is reduced to four.

An illustrative way to arrive at the definition of staggered fermions is the so-called spin diagonalization. We consider a unitary local matrix A_x , acting in Dirac space, that transforms the spinors $\bar{\psi}_x$ and ψ_x such that the Dirac matrices can be written as a product of phase factors times a unit matrix

$$\begin{aligned}\psi_x &= A_x \chi_x, \\ \bar{\psi}_x &= \bar{\chi}_x A_x^\dagger.\end{aligned}\quad (2.42)$$

Inserting this into the naive action (2.39) one obtains

$$S_F = a^4 \left\{ \frac{1}{2a} \sum_{x,\mu} \left[\bar{\chi}_x \Delta_{x\mu} U_{x\mu} \chi_{x+\hat{\mu}} - \bar{\chi}_{x+\hat{\mu}} \Delta_{x\mu}^\dagger U_{x\mu}^\dagger \chi_x \right] + m \sum_x \bar{\chi}_x \chi_x \right\}, \quad (2.43)$$

with

$$\begin{aligned}\Delta_{x\mu} &= A_x^\dagger \gamma_\mu A_{x+\hat{\mu}}, \\ \Delta_{x\mu}^\dagger &= A_{x+\hat{\mu}}^\dagger \gamma_\mu A_x.\end{aligned}\quad (2.44)$$

We require

$$\Delta_{x\mu} = \Gamma_{x\mu} 1. \quad (2.45)$$

One possible choice to fulfill this requirement is

$$\begin{aligned}A_x &= \gamma_1^{x_1} \gamma_2^{x_2} \gamma_3^{x_3} \gamma_4^{x_4}, \\ A_x^\dagger &= \gamma_4^{x_4} \gamma_3^{x_3} \gamma_2^{x_2} \gamma_1^{x_1}.\end{aligned}\quad (2.46)$$

One obtains

$$\Delta_{x\mu} = (-1)^{x_1 + \dots + x_{\mu-1}} 1 =: \Gamma_{x\mu} 1 \quad (2.47)$$

and

$$\Delta_{x\mu}^\dagger = \Delta_{x\mu}. \quad (2.48)$$

Other possible matrices A'_x can be calculated from unitary transformations of A_x .

The diagonalized action S_F is

$$a^4 \left\{ \frac{1}{2a} \sum_{x,\mu} \Gamma_{x\mu} \left[\bar{\chi}_{x,\alpha}^c 1_{\alpha\beta} U_{x\mu}^{cc'} \chi_{x+\hat{\mu},\beta}^{c'} - \bar{\chi}_{x+\hat{\mu},\alpha}^c 1_{\alpha\beta} U_{x\mu}^{\dagger cc'} \chi_{x,\beta}^{c'} \right] + m \sum_x \bar{\chi}_{x,\alpha}^c \chi_{x,\alpha}^c \right\}, \quad (2.49)$$

with the Dirac indices $\alpha, \beta = 1, \dots, 4$ and the color indices $c, c' = 1, 2, 3$.

Because of the unit matrix between the spinors (2.49) consists of four identical terms. The dynamics of the system is completely described by a single term. Neglecting the others the degeneracy is reduced to four. This leads to the following, Kogut-Susskind, action

$$S_F = a^4 \left\{ \frac{1}{2a} \sum_{x,\mu} \Gamma_{x\mu} \left[\bar{\chi}_x U_{x\mu} \chi_{x+\hat{\mu}} - \bar{\chi}_{x+\hat{\mu}} U_{x\mu}^\dagger \chi_x \right] + m \sum_x \bar{\chi}_x \chi_x \right\}, \quad (2.50)$$

where χ_x^c and $\bar{\chi}_x^c$ are one component fields in Dirac space.

For $m = 0$ the reduced action is invariant with respect to the global transformations

$$\left. \begin{aligned} \chi_x &\rightarrow e^{i\alpha} \chi_x \\ \bar{\chi}_x &\rightarrow e^{-i\beta} \bar{\chi}_x \end{aligned} \right\} \text{for } (-1)^{x_1+x_2+x_3+x_4} = 1$$

$$\left. \begin{aligned} \chi_x &\rightarrow e^{i\beta} \chi_x \\ \bar{\chi}_x &\rightarrow e^{-i\alpha} \bar{\chi}_x \end{aligned} \right\} \text{for } (-1)^{x_1+x_2+x_3+x_4} = -1, \quad (2.51)$$

where α and β are independent phases. This residual symmetry originates from the chiral symmetry of the continuum action and ensures that no counter terms are needed for renormalization (that means $m_{\text{bare}} = 0$ implies $m_{\text{ren}} = 0$).

Due to the partial conservation of chiral symmetry the degeneracy could not be completely avoided, as was mentioned above in this section. In practice one introduces a factor $\frac{1}{4}$ in the action to account for the remaining degeneracy. Whether this concept gives the correct continuum limit is an unsolved problem. Additionally, it is difficult to construct baryonic operators with well defined quantum numbers. Although the Kogut-Susskind or staggered scheme provides an elegant discretization method, its physical meaning is not yet fully enlightened.

Wilson Fermions

To avoid fermion doubling, in this method an extra term [8]

$$ra^4 \sum_x \sum_\mu \frac{1}{2a} (\bar{\psi}_{x+\hat{\mu}} - \bar{\psi}_x)(\psi_{x+\hat{\mu}} - \psi_x) \quad (2.52)$$

is added to the naive action (2.38), where $0 < r \leq 1$ is a free parameter [12, 13]. This term is of order $\mathcal{O}(a^5)$

$$ra^4 \sum_x \sum_\mu \frac{1}{2a} a\bar{\psi}'_x a\psi'_x \sim \mathcal{O}(a^5) \quad (2.53)$$

and vanishes in the classical continuum limit, relative to the rest of the action, which is of order $\mathcal{O}(a^4)$.

The new action becomes

$$S_F = a^4 \left\{ \frac{1}{2a} \sum_{x,\mu} \left(\bar{\psi}_x \gamma_\mu \psi_{x+\hat{\mu}} - \bar{\psi}_{x+\hat{\mu}} \gamma_\mu \psi_x + r \bar{\psi}_{x+\hat{\mu}} \psi_{x+\hat{\mu}} + r \bar{\psi}_x \psi_x - r \bar{\psi}_{x+\hat{\mu}} \psi_x - r \bar{\psi}_x \psi_{x+\hat{\mu}} \right) + m \sum_x \bar{\psi}_x \psi_x \right\}. \quad (2.54)$$

Using

$$\begin{aligned} \frac{1}{2a} \sum_x \sum_\mu \bar{\psi}_x \psi_x &= \frac{2}{a} \sum_x \bar{\psi}_x \psi_x, \\ \frac{1}{2a} \sum_x \sum_\mu \bar{\psi}_{x+\hat{\mu}} \psi_{x+\hat{\mu}} &= \frac{2}{a} \sum_x \bar{\psi}_x \psi_x, \end{aligned} \quad (2.55)$$

and rescaling the fields

$$\begin{aligned} \psi &\rightarrow \left[a^3 (4r + ma) \right]^{-1/2} \psi, \\ \bar{\psi} &\rightarrow \left[a^3 (4r + ma) \right]^{-1/2} \bar{\psi}, \end{aligned} \quad (2.56)$$

one obtains

$$S_F = -\kappa \sum_{x,\mu} \left[\bar{\psi}_x (r - \gamma_\mu) \psi_{x+\hat{\mu}} + \bar{\psi}_{x+\hat{\mu}} (r + \gamma_\mu) \psi_x \right] + \sum_x \bar{\psi}_x \psi_x, \quad (2.57)$$

with the hopping parameter

$$\kappa = \frac{1}{8r + 2ma}. \quad (2.58)$$

Defining the fermionic matrix

$$M_{xx'} = \delta_{xx'} - \kappa Q_{xx'} \quad (2.59)$$

with

$$Q_{xx'} = \sum_\mu \left[(r - \gamma_\mu) \delta_{x+\hat{\mu},x'} + (r + \gamma_\mu) \delta_{x,x'+\hat{\mu}} \right], \quad (2.60)$$

the corresponding fermion propagator turns out to be

$$G(p) = \widetilde{M}^{-1}(p) \propto \frac{1}{m + \frac{i}{a} \sum_\mu \sin(p_\mu a) + \frac{r}{a} \sum_\mu (1 - \cos(p_\mu a))}. \quad (2.61)$$

The originally degenerate particles acquire an additional mass on the former poles from the Wilson term

$$p_\mu a = \begin{cases} (\pi, 0, 0, 0) , \dots , (0, 0, 0, \pi) & m + \frac{2r}{a} \\ (\pi, \pi, 0, 0) , \dots , (0, 0, \pi, \pi) & m + \frac{4r}{a} \\ (\pi, \pi, \pi, 0) , \dots , (0, \pi, \pi, \pi) & m + \frac{6r}{a} \\ (\pi, \pi, \pi, \pi) & m + \frac{8r}{a} . \end{cases} \quad (2.62)$$

These states have an infinite mass in the limit $a \rightarrow 0$ and vanish from the spectrum. The degeneracy is completely removed.

The diagonal parts of the Wilson term correspond to an additional mass term, which breaks the chiral symmetry explicitly. This means that even for $m = 0$ the Lagrangian is not invariant under chiral transformations.

The additional mass term also gives rise to mass counter terms in the renormalization process. Therefore, a vanishing bare mass m_0 does not generally lead to a renormalized mass $m_{\text{ren}} = 0$. This is a fundamental difference to the Kogut-Susskind method. As a consequence the non-renormalized mass parameter in the staggered action and the bare mass in the hopping parameter of the Wilson action are not identical. Therefore a direct comparison of the two methods is not easy to accomplish. In contrast to the Kogut-Susskind action, the Wilson action shows the correct continuum limit.

2.1.6 Monopoles and Confinement

The $U(1)$ plaquette angles $\theta_{x,\mu\nu} \equiv U_{x,\mu\nu}$ can be decomposed into the ‘‘physical’’ electromagnetic flux through the plaquette $\bar{\theta}_{x,\mu\nu}$ and a number $m_{x,\mu\nu}$ of Dirac strings passing through the plaquette

$$\theta_{x,\mu\nu} = \bar{\theta}_{x,\mu\nu} + 2\pi m_{x,\mu\nu} , \quad (2.63)$$

where $\bar{\theta}_{x,\mu\nu} \in (-\pi, +\pi]$. One calls plaquettes with $m_{x,\mu\nu} \neq 0$ *Dirac plaquettes*. The monopole charges in elementary $3d$ cubes are defined as the net number of Dirac strings entering or exiting these cubes. The worldlines of these monopoles on the dual lattice are closed, either within the lattice volume or by the periodic boundary conditions.

The relation between confinement and dual superconductivity of the ground state of gauge theories has been analyzed in many studies [20, 21]. Monopoles exist in gauge theories, carrying a conserved magnetic charge. A disorder parameter $\langle \mu \rangle$ can be defined for detecting dual superconductivity as spontaneous breaking of the $U(1)$ symmetry related to magnetic charge conservation. $\langle \mu \rangle \neq 0$ signals that the ground state is a superposition of states with different magnetic

charge, a phenomenon which is denoted as condensation and which implies dual superconductivity under very general assumptions.

In $SU(2)$ a monopole species can be associated to any operator in the adjoint representation, with a corresponding magnetic $U(1)$ symmetry. Condensation can be numerically investigated for different monopole species, in connection with confinement, by lattice simulation at finite temperature. The main results of the investigation for $SU(2)$ were the following: Monopoles defined by different Abelian projections do condense in the confined phase, $\langle \mu \rangle \neq 0$, whereas at deconfinement $\langle \mu \rangle \rightarrow 0$. All the monopole species considered have a similar behavior, and show dual superconductivity. The analysis was also extended to $SU(3)$ gauge group and the essentials are not changed with respect to $SU(2)$.

2.1.7 Finite Temperature on the Lattice

It is assumed that at very high temperatures QCD undergoes a phase transition from the confinement to the deconfinement phase [8]. There, quarks and gluons are free particles in, what is called, the quark-gluon plasma. Especially in high energy physics and in cosmology one is interested in an investigation of the phase transition and the properties of the quark-gluon plasma. For this purpose a definition of QCD at finite temperatures is needed.

For a pointlike quantum mechanical particle, described by a Hamiltonian H , in a heat bath of temperature $T \equiv \frac{1}{\beta_B}$ the partition function is

$$Z = \text{Tr} e^{-\beta_B H} . \quad (2.64)$$

Evaluating Z in coordinate space gives

$$Z = \int dx \langle x | e^{-\beta_B H} | x \rangle . \quad (2.65)$$

In the path integral formalism the partition function is given by

$$Z = \sum_{\text{periodic paths}} \exp \left(- \int_0^{\beta_B} dx_4 \mathcal{L}^E(x_4) \right) , \quad (2.66)$$

where one has to sum over all paths fulfilling $x(\beta_B) = x(0)$.

Generalizing this for lattice QCD gives

$$Z = \int \mathcal{D}[U, \psi, \bar{\psi}] e^{-(S_G + S_F)} , \quad (2.67)$$

where the fields have to be periodic in time. This means periodic boundary conditions for gauge fields and anti-periodic boundary conditions for the quark fields, because they are Grassmann variables. Additionally the thermodynamic limit has to be performed for the lattice with the extent $N_x \times N_y \times N_z \times N_t$, that means $V = N_x a N_y a N_z a \rightarrow \infty$, where the time extent $N_t a$ has to be kept fixed. The temperature $T = \frac{1}{N_t a}$ is given by the inverse time extent of the lattice. Since the lattice constant a depends on the coupling constant g , the temperature can be controlled via the inverse coupling constant $\beta = \frac{6}{g^2}$. Thermodynamic observables can be calculated as usual as derivatives of the partition function with respect to temperature, volume and so on.

2.1.8 Numerical Simulation

The aim of numerical simulations is to calculate expectation values [22]

$$\langle O \rangle = \frac{\int \mathcal{D}[U, \bar{\psi}, \psi] O(U, \bar{\psi}, \psi) e^{-S[U, \bar{\psi}, \psi]}}{\int \mathcal{D}[U, \bar{\psi}, \psi] e^{-S[U, \bar{\psi}, \psi]}}. \quad (2.68)$$

In pure gluonic QCD (2.68) is reduced to

$$\langle O \rangle = \frac{1}{Z} \int \mathcal{D}[U] O(U) e^{-S[U]}. \quad (2.69)$$

On an N^4 lattice with $SU(3)$ gauge symmetry one has to evaluate $32N^4$ integrals over the generalized Euler angles. Even for small lattices it is impossible to perform such a number of integrals numerically. Fortunately, it is not necessary to do that as it is sufficient to consider a small number of representative configurations which are those with the largest statistical weight. The largest statistical weight is given by the minimal action as for the minimal action the Boltzmann factor e^{-S} is large. The path integral (2.69), therefore, becomes an averaging over these configurations

$$\langle O \rangle = \frac{1}{N_{\text{Konf}}} \sum_{i=1}^{N_{\text{Konf}}} O(\{U\}_i). \quad (2.70)$$

This approximation converges to the exact integral in the limit of a large number of independent configurations. The factor e^{-S} does not appear in (2.70) as it is taken into account in the generation of the configurations. The main purpose is, therefore, to generate as many independent configurations with minimal action as possible.

Monte Carlo Method

Let Σ denote a configuration of the gauge field U [22]. In equilibrium the configurations are generated with a probability $P(\Sigma)$ proportional to their statistical weight

$$P(\Sigma) \propto e^{-S(\Sigma)} . \quad (2.71)$$

Such configurations can be generated by a discrete Markov process, i.e. each configuration of the Markov chain is generated from the preceding configuration and they are independent from each other.

Let $P(\Sigma \rightarrow \Sigma')$ denote the transition probability from the configuration Σ to the configuration Σ' . $P(\Sigma \rightarrow \Sigma')$ has to fulfill the following requirements:

- Each configuration with a finite action has to be reached in finite number of steps

$$P(\Sigma \rightarrow \Sigma') > 0 , \text{ for each } \Sigma, \Sigma' . \quad (2.72)$$

- The sum of the transition probability from one configuration to any other configuration has to be 1

$$\sum_{\Sigma'} P(\Sigma \rightarrow \Sigma') = 1 . \quad (2.73)$$

- Detailed balance should exist

$$\frac{P(\Sigma \rightarrow \Sigma')}{P(\Sigma' \rightarrow \Sigma)} = \frac{e^{-S(\Sigma')}}{e^{-S(\Sigma)}} . \quad (2.74)$$

If these restrictions are fulfilled each chain reaches an equilibrium in a finite number of steps. In the equilibrium the probability of finding configuration Σ is given by (2.71). The expectation value of an observable O in the detailed balance is given by

$$\langle O \rangle = \frac{1}{N_\Sigma} \sum_{i=1}^{N_\Sigma} O(\Sigma_i) . \quad (2.75)$$

Metropolis Algorithm

Considering the gauge field element U which is situated on a specified link of the lattice [22]. U is then multiplied by a random matrix $V \in SU(3)$ which is close to unity. The probability for the multiplication with V has to be equal to the probability for the multiplication with the inverse

$$p(V) = p(V^\dagger) . \quad (2.76)$$

If the action decreases the old gauge field element U is replaced by VU . If the action increases it depends on a random number r whether or not U is replaced. Therefore,

$$e^{-[S(VU)-S(U)]} - r \begin{cases} \geq 0 \Rightarrow U' = VU \\ < 0 \Rightarrow U' = U, \end{cases} \quad (2.77)$$

where r is a uniformly distributed random number from the interval $[0, 1]$. Supposing the gauge field is only replaced if the action decreases then the system would converge to the classical limit and all quantum fluctuations were suppressed. One also prevents to fall in a local minimum by using this implementation. If the action increases $S(U') > S(U)$ then

$$\begin{aligned} P(U \rightarrow U') &= p(V)e^{-(S(U')-S(U))}, \\ P(U' \rightarrow U) &= p(V^\dagger), \end{aligned} \quad (2.78)$$

and with $p(V) = p(V^\dagger)$ follows

$$\frac{P(U \rightarrow U')}{P(U' \rightarrow U)} = \frac{e^{-S(U')}}{e^{-S(U)}}. \quad (2.79)$$

2.2 Lyapunov Exponent in U(1) and SU(2) Gauge Theory

The study of chaotic dynamics of classical field configurations in field theory finds its motivation in phenomenological applications as well as for the understanding of basic principles. The role of chaotic field dynamics for the confinement of quarks is a longstanding question. Here, we analyze the leading Lyapunov exponents of compact $U(1)$ and of $SU(2)$ -Yang-Mills field configurations on the lattice. The real-time evolution of the classical field equations was initialized from Euclidean equilibrium configurations created by quantum Monte Carlo simulations. This way we expect to see a coincidence between the strong coupling phase and the strength of chaotic behavior in lattice simulations [23].

2.2.1 Classical Chaotic Dynamics

Chaotic dynamics in general is characterized by the spectrum of Lyapunov exponents. These exponents, if they are positive, reflect an exponential divergence of initially adjacent configurations. In case of symmetries inherent in the Hamiltonian of the system there are corresponding zero values of these exponents. Finally negative exponents belong to irrelevant directions in the phase space: perturbation components in these directions die out exponentially. Pure gauge fields on the lattice show a characteristic Lyapunov spectrum consisting of one third of each kind of exponents [24]. This fact reflects the elimination of longitudinal degrees of freedom of the gauge bosons. Assuming this general structure of the Lyapunov spectrum we investigate presently its magnitude only, namely the maximal value of the Lyapunov exponent, L_{\max} .

The general definition of the Lyapunov exponent is based on a distance measure $d(t)$ in phase space,

$$L := \lim_{t \rightarrow \infty} \lim_{d(0) \rightarrow 0} \frac{1}{t} \ln \frac{d(t)}{d(0)}. \quad (2.80)$$

In case of conservative dynamics the sum of all Lyapunov exponents is zero according to Liouville's theorem,

$$\sum L_i = 0. \quad (2.81)$$

We utilize the gauge invariant distance measure consisting of the local differences of energy densities between two field configurations on the lattice:

$$d := \frac{1}{N_P} \sum_P |\text{tr}U_P - \text{tr}U'_P|. \quad (2.82)$$

Here the symbol \sum_P stands for the sum over all N_P plaquettes, so this distance is bound in the interval $(0, 2N)$ for the group $SU(N)$. U_P and U'_P are the familiar plaquette variables, constructed from the basic link variables $U_{x,i}$,

$$U_{x,i} = \exp(aA_{x,i}^c T^c), \quad (2.83)$$

located on lattice links pointing from the position $x = (x_1, x_2, x_3)$ to $x + ae_i$. The generators of the group are $T^c = -ig\tau^c/2$ with τ^c being the Pauli matrices in case of $SU(2)$ and $A_{x,i}^c$ is the vector potential. The elementary plaquette variable is constructed for a plaquette with a corner at x and lying in the ij -plane as

$$U_{x,ij} = U_{x,i} U_{x+i,j} U_{x+j,i}^\dagger U_{x,j}^\dagger. \quad (2.84)$$

It is related to the magnetic field strength $B_{x,k}^c$:

$$U_{x,ij} = \exp(\varepsilon_{ijk} a B_{x,k}^c T^c). \quad (2.85)$$

The electric field strength $E_{x,i}^c$ is related to the canonically conjugate momentum $P_{x,i} = \dot{U}_{x,i}$ via

$$E_{x,i}^c = \frac{2a}{g^3} \text{tr} \left(T^c \dot{U}_{x,i} U_{x,i}^\dagger \right). \quad (2.86)$$

2.2.2 Initial States Prepared by Quantum Monte Carlo

The Hamiltonian of the lattice gauge field system can be casted into the form

$$H = \sum \left[\frac{1}{2} \langle P, P \rangle + 1 - \frac{1}{4} \langle U, V \rangle \right]. \quad (2.87)$$

Here the scalar product between group elements stands for $\langle A, B \rangle = \frac{1}{2} \text{tr}(AB^\dagger)$. The staple variable V is a sum of triple products of elementary link variables closing a plaquette with the chosen link U . This way the Hamiltonian is formally written as a sum over link contributions and V plays the role of the classical force acting on the link variable U . The naive equations of motion following from this Hamiltonian, however, have to be completed in order to fulfill the constraints

$$\begin{aligned} \langle U, U \rangle &= 1, \\ \langle P, U \rangle &= 0. \end{aligned} \quad (2.88)$$

The following finite time step recursion formula:

$$\begin{aligned} U' &= U + dt(P' - \varepsilon U), \\ P' &= P + dt(V - \mu U + \varepsilon P'), \end{aligned} \quad (2.89)$$

with the Lagrange multipliers

$$\begin{aligned}\varepsilon &= \langle U, P' \rangle, \\ \mu &= \langle U, V \rangle + \langle P', P' \rangle,\end{aligned}\tag{2.90}$$

conserves the Noether charge belonging to the Gauss law,

$$\Gamma = \sum_{+} PU^{\dagger} - \sum_{-} U^{\dagger}P.\tag{2.91}$$

Here the sums indicated by $+$ run over links starting from, and those by $-$ ending at a given site x , where the Noether charge Γ is defined. The above algorithm is written in an implicit form, but it can be casted into explicit steps, so no iteration is necessary [25].

Initial conditions chosen randomly with a given average magnetic energy per plaquette have been investigated in past years. In the $SU(2)$ case, a linear scaling of the maximal Lyapunov exponent with the total energy of the system has been established for different lattice sizes and coupling strengths [24]. In the present study we prepare the initial field configurations from a standard four dimensional Euclidean Monte Carlo program on a $12^3 \times 4$ lattice varying the inverse gauge coupling β [26].

We relate such four dimensional Euclidean lattice field configurations to Minkowskian momenta and fields for the three dimensional Hamiltonian simulation by the following approach:

First we fix a time slice of the four dimensional lattice. We denote the link variables in the three dimensional sub-lattice by $U' = U_i(x, t)$. Then we build triple products on attached handles in the positive time direction, $U'' = U_4(x, t)U_i(x, t + a)U_4^{\dagger}(x + a, t)$. We obtain the canonical variables of the Hamiltonian system by using

$$\begin{aligned}P &= (U'' - U')/dt, \\ U &\propto (U'' + U').\end{aligned}\tag{2.92}$$

Finally U is normalized to $\langle U, U \rangle = 1$.

This definition constructs the momenta according to a simple definition of the time-like covariant derivative. The multiplication with the link variables in time direction can also be viewed as a gauge transformation to $U_4(x, t) = 1$, i.e. $A_0 = 0$ Hamiltonian gauge.

Sonification Results

3.1 Dirac Operator for Fixed Beta

For the first sonification in lattice field theory we took the eigenvalue spectrum of the Dirac operator from existing data [27]. There the gauge field configurations were generated using the standard Wilson plaquette action for $SU(3)$ and the matrix of the Dirac operator was constructed using the Kogut-Susskind prescription (2.50). The Dirac matrix is anti-hermitian so that all eigenvalues are imaginary and occur in pairs with opposite sign. We work on a $6^3 \times 4$ lattice with various values of the coupling strength β . Typically there have been 10 independent configurations for each value of β . In the first sonification attempt the spectra for ascending eigenvalues keeping β fixed were analyzed [28].

Fig. 3.1 shows a graphical presentation of the 15 lowest eigenvalues from $\beta = 5.0$ to $\beta = 6.0$. The phase transition to deconfinement occurs around $\beta = 5.7$ where all quasi-zero modes vanish.

To prepare the input data for sonification we multiplied the raw data by a factor of 10000 and added the standard pitch of 440 Hz. The outcome is shown in Fig. 3.2 for the spectra from the confinement to the deconfinement phase.

For the sonification process we wrote a slang program similar to the program code of another sonification project treating baryon spectra obtained from different constituent quark models [7]. In Fig. 3.3 we present screenshots of the 15 lowest eigenvalues for $\beta = 5.0$ and $\beta = 6.0$. Listening to the sound files one can hear that the melody is rather similar for the β -values in the **confinement**

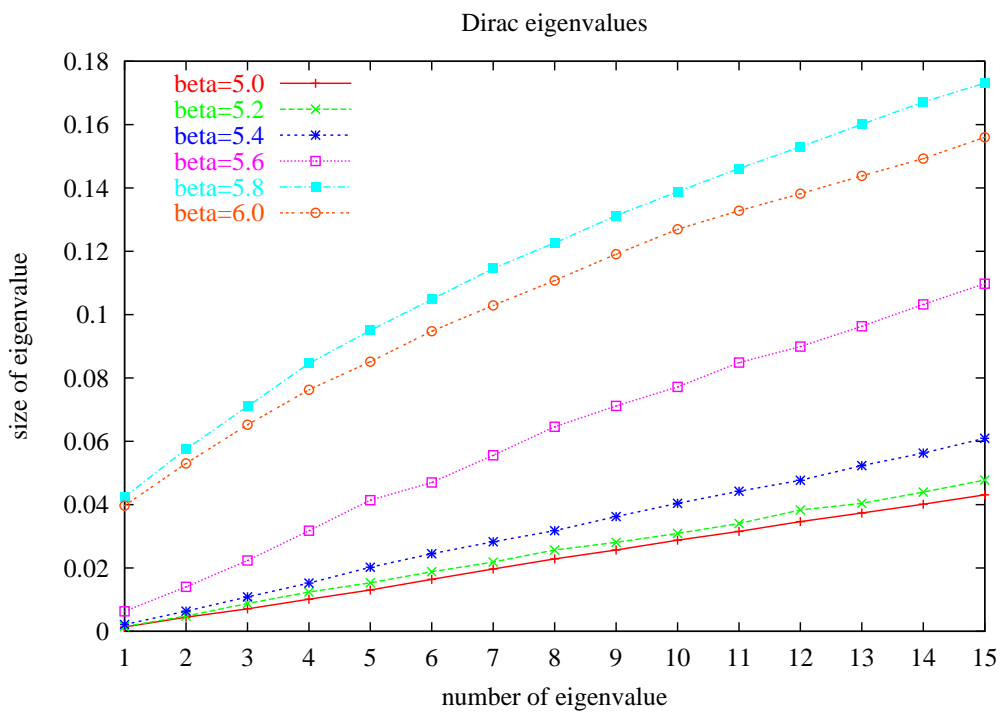


Figure 3.1 Configuration-averaged values of the 15 lowest levels of the eigenvalue spectrum of the Dirac operator for 6 different couplings β .

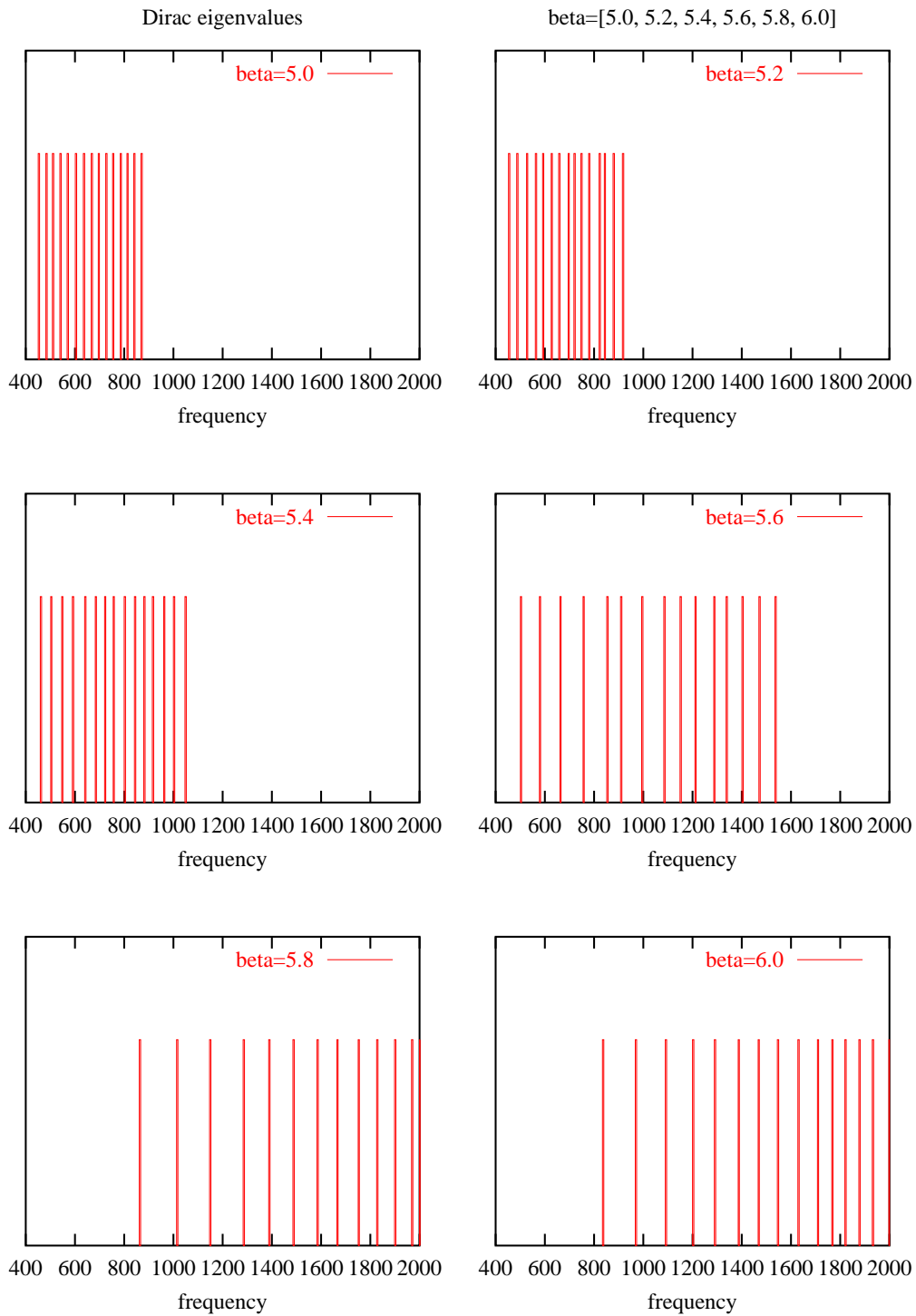


Figure 3.2 Eigenvalue spectra transformed into audible region for β -values across the phase transition from quark confinement to the quark-gluon plasma.



Figure 3.3 Screenshots of the low-lying part of the spectrum of the Dirac operator in the confinement and deconfinement region.

phase [web/cdrom] with a slight increase towards higher coupling. The quasi-zero mode of the lowest eigenvalue stays around 440 Hz. After the transition to the deconfinement region [web/cdrom] the sound changes clearly to higher tones. The lowest eigenvalue starts above 800 Hz. This means that one can hear the restoration of chiral symmetry when increasing the coupling to the quark-gluon plasma-phase. These sample results are stored on the SonEnvir server and can be accessed there [29].

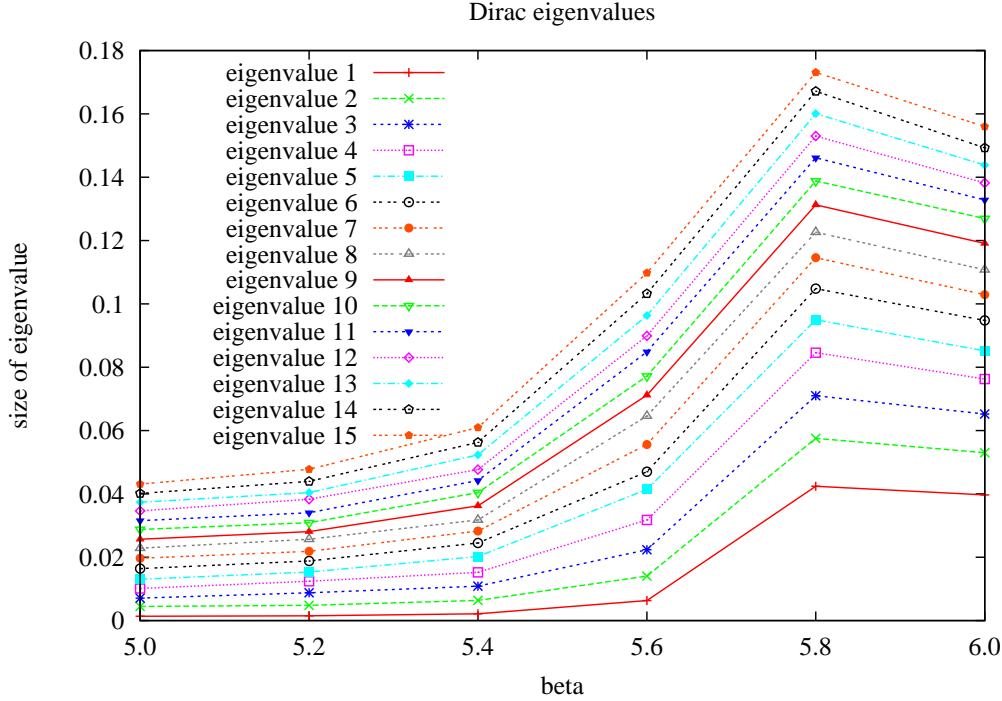


Figure 3.4 Configuration-averaged values of the 15 lowest levels of the eigenvalue spectrum of the Dirac operator as a function of the gluon coupling β .

3.2 Dirac Operator as a Function of Beta

This sonification example is similar to the first one. But now we performed a sonification keeping the eigenvalue fixed as a function of the coupling β [30].

Fig. 3.4 shows a graphical presentation of the 15 lowest eigenvalues as a function of the gluon coupling from $\beta = 5.0$ to $\beta = 6.0$. The phase transition to deconfinement occurs around $\beta = 5.7$ where the quasi-zero modes disappear. One observes that all eigenvalues independent of their topological content are influenced at the transition point.

For the audio files we again multiplied the raw data by a factor of 10000 and added the standard pitch of 440 Hz. In Fig. 3.5 we depict the frequencies obtained for the eigenvalue numbers 1,2,3,5,10 and 15 from the confinement to the deconfinement phase.

In Fig. 3.6 we present screenshots of the 1st eigenvalue [web/cdrom] and the 10th eigenvalue [web/cdrom] from $\beta = 5.0$ to $\beta = 6.0$. Listening to the sound files one can hear that the melody is changing clearly to higher tones around the

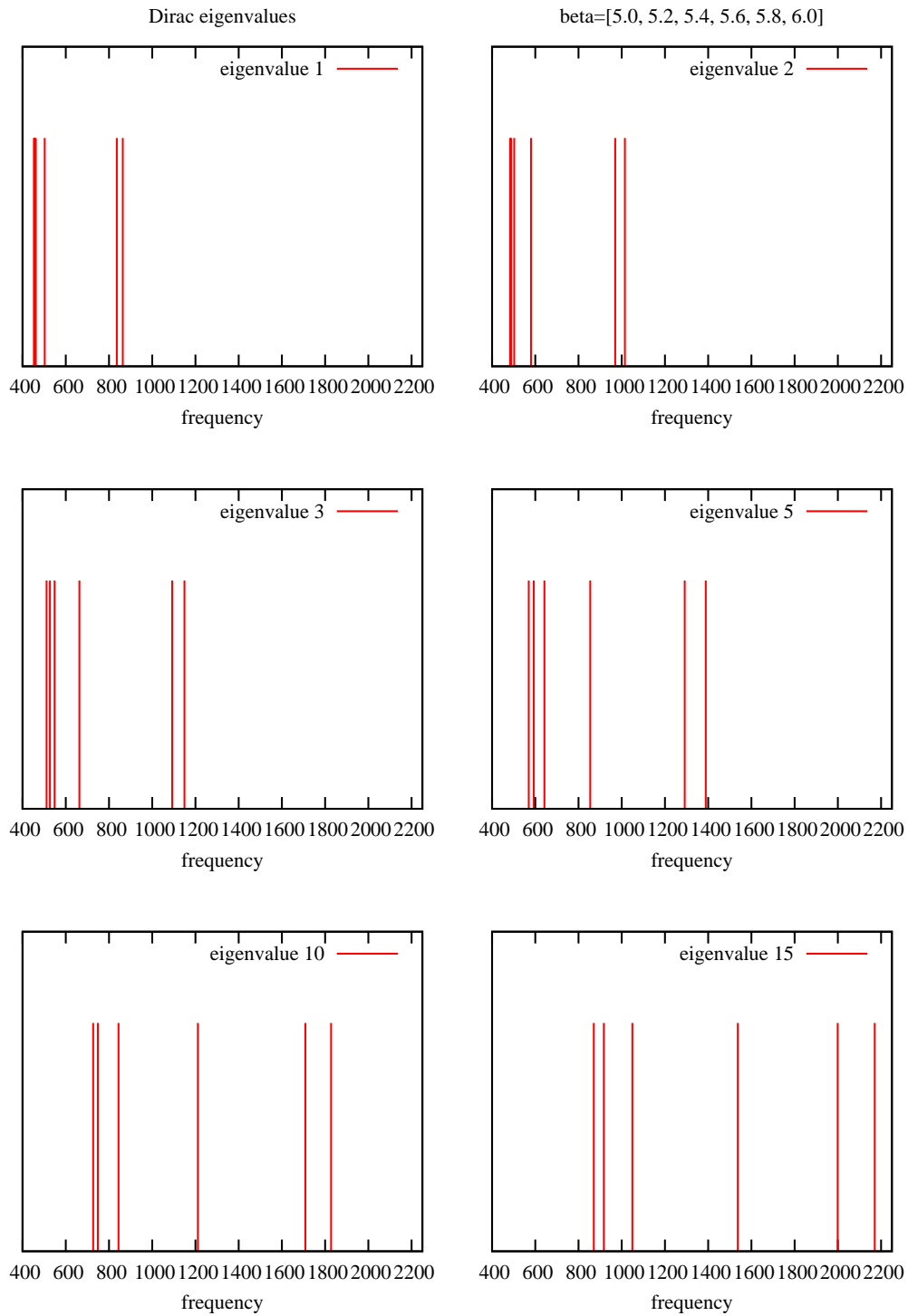


Figure 3.5 Six selected eigenvalues transformed into the audible region for values of β across the QCD phase transition.



Figure 3.6 Screenshots of the lowest and the 10th eigenvalue of the Dirac operator moving from the confinement to the deconfinement region.

critical β -value. Both eigenvalue sequences behave similarly. Only the quasi-zero mode of the lowest eigenvalue starts around 440 Hz whereas the higher eigenvalue begins correspondingly higher. This means that one can hear the restoration of chiral symmetry when increasing the coupling beyond the phase transition to the quark-gluon plasma. These sample results can also be found on the SonEnvir server [29].

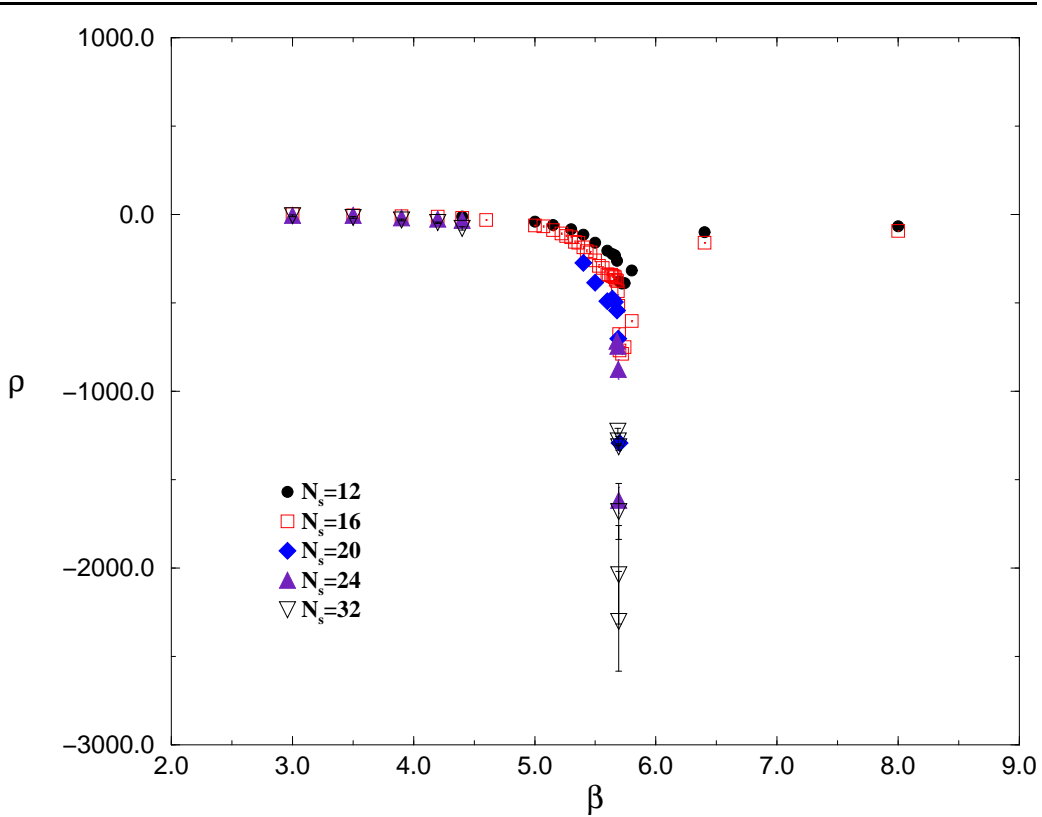


Figure 3.7 Monopole disorder parameter ρ computed by the Pisa group as a function of β for different spatial sizes at fixed $N_t = 4$ with Polyakov projection and Abelian generator F^3 .

3.3 Disorder Parameter for Magnetic Monopoles

When crossing the transition point to the quark-gluon plasma the topological charge and the monopole density exhibit drastic changes and disappear. The Pisa group developed and computed a (dis)order parameter for magnetic monopoles on the lattice. Fig. 3.7 displays the derivative of the logarithmic monopole density with respect to β for $SU(3)$ gauge theory. The kink of the monopole density is thus transformed to a clearly visible spike, which becomes more pronounced with increasing lattice size and stays practically independent of the Abelian projection [21].

In Fig. 3.8 we display snapshots of the disorder parameter ρ around $\beta = 4$ and at the critical point $\beta = 5.7$ for spatial lattice size $N_s = 16$, the left showing exactly one frequency whereas the right exhibits a bunch of frequencies from the



Figure 3.8 Snapshots of the zero-value at small couplings and of the spike of the monopole disorder parameter at the transition point.

sharp dip [31]. The sound file presents ρ [web/cdrom] for varying β with the melody changing clearly to lower tones around criticality. This means that one can hear the phase transition to the quark-gluon plasma where the monopoles vanish. These sample results can be accessed from the SonEnvir server [29].

3.4 Lyapunov Exponent in $U(1)$ and $SU(2)$ Theory

The numerical computation of the Lyapunov exponents in gauge theories was carried out in the course of this thesis. At first we show a characteristic example of the time evolution of the distance between initially adjacent configurations. An initial state prepared by a standard four dimensional Monte Carlo simulation is evolved according to the classical Hamiltonian dynamics in real time. Afterwards this initial state is rotated locally by group elements which are chosen randomly near to the unity. The time evolution of this slightly rotated configuration is then pursued and finally the distance between these two evolutions is calculated at the corresponding times. A typical exponential rise of this distance followed by a saturation can be inspected in Fig. 3.9 from an example of $U(1)$ gauge theory in the confinement phase and in the Coulomb phase [23]. While the saturation is an artifact of the compact distance measure of the lattice, the exponential rise (the linear rise of the logarithm) can be used for the determination of the leading Lyapunov exponent. The naive determination and more sophisticated rescaling methods lead to the same result.

The dependence of the leading Lyapunov exponent L_{\max} on the inverse coupling strength β is displayed in Fig. 3.10 for a statistics of 100 independent $U(1)$ configurations. As expected the strong coupling phase, where confinement of static sources has been established many years ago by proving the area law behavior for large Wilson loops, is more chaotic. The transition reflects the critical coupling to the Coulomb phase. Furthermore the maximal Lyapunov exponent scatters more pronounced than the average energy per plaquette. Fig. 3.11 shows the somewhat smoother transition of the energy per plaquette as a function of the inverse coupling strength. Fig. 3.12 depicts the correlation of the Lyapunov exponents and the plaquette energies for 100 $U(1)$ configurations. The blank area is indicative of the transition point being presumable of first order.

Next we turn to the comparison of expectation values of $U(1)$ and $SU(2)$ theory. Fig. 3.13 exhibits the averaged leading Lyapunov exponent between the strong and the weak coupling regime. The smoother fall-off of the $SU(2)$ Lyapunov exponent reflects the second order of the finite temperature transition to a Debye screened phase of free quarks. Fig. 3.14 compares the averaged plaquette energies of both gauge theories signaling the different order of their phase transitions.

Fig. 3.15 shows the energy dependence of the Lyapunov exponents for both theories. One observes an approximately linear relation for the $SU(2)$ case while a quadratic relation is suggested for the $U(1)$ theory in the weak coupling regime. From scaling arguments a functional relationship between the Lyapunov exponent

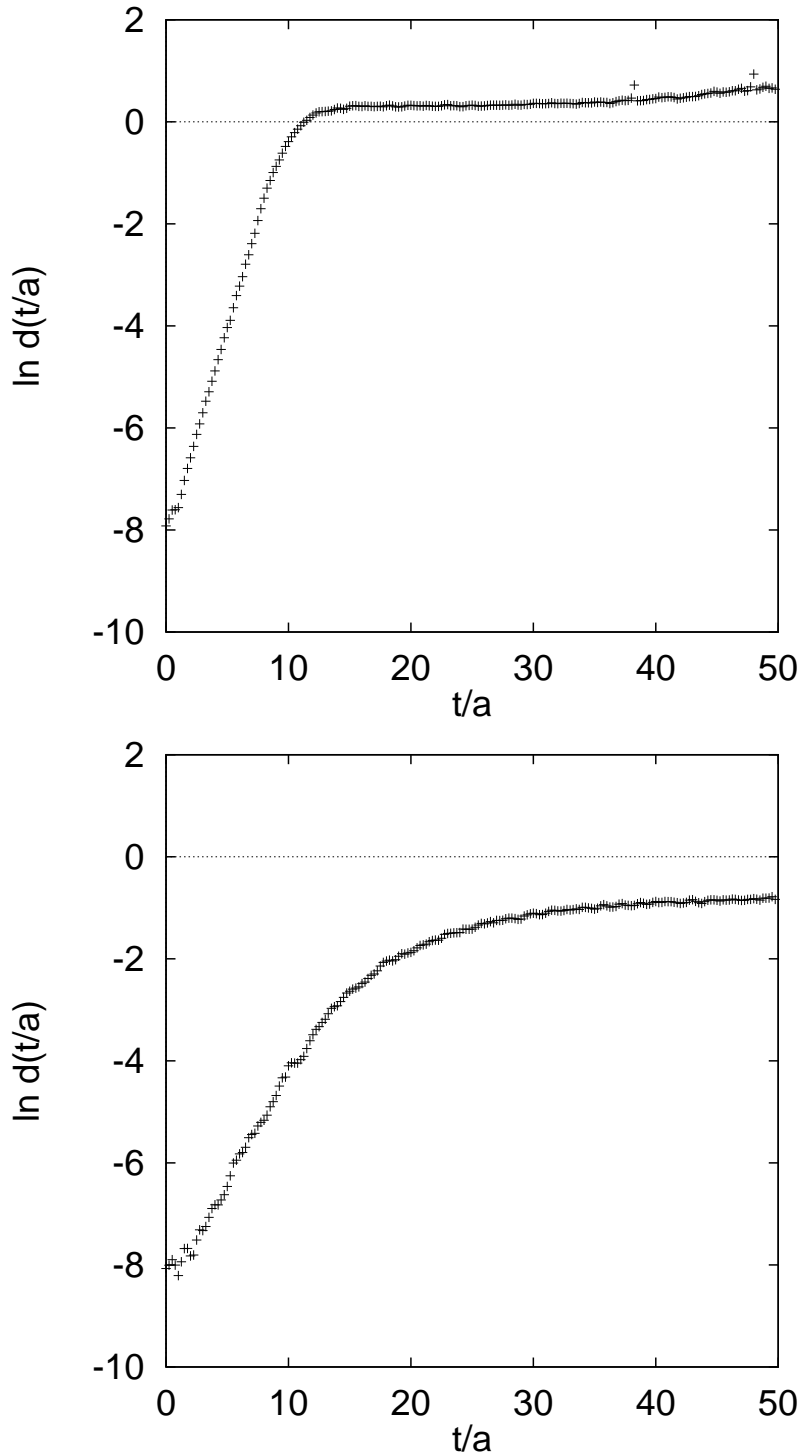


Figure 3.9 Exponentially diverging distance of initially adjacent $U(1)$ field configurations on a 12^3 lattice prepared at $\beta = 0.9$ in the confinement phase (top) and at $\beta = 1.1$ in the Coulomb phase (bottom).

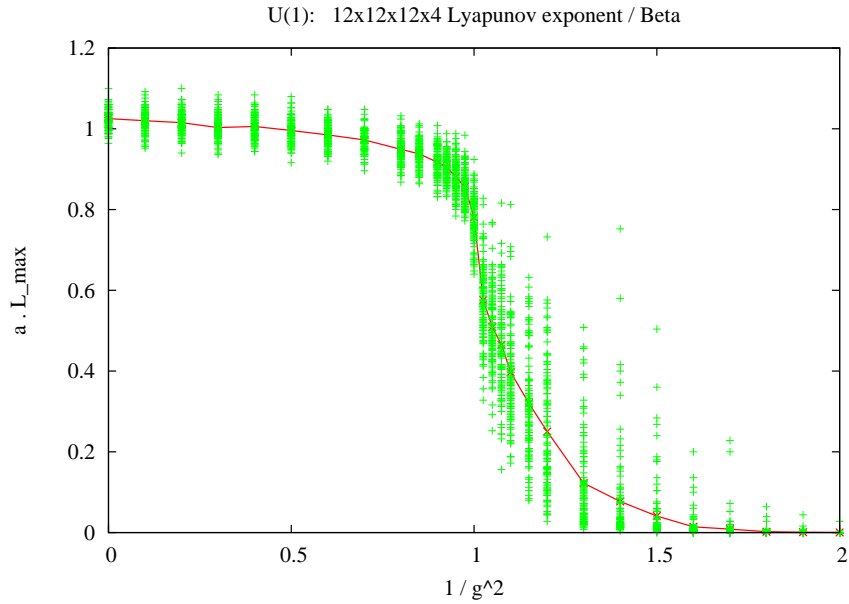


Figure 3.10 Transition of the leading Lyapunov exponents from 100 $U(1)$ configurations as a function of the inverse coupling strength β .

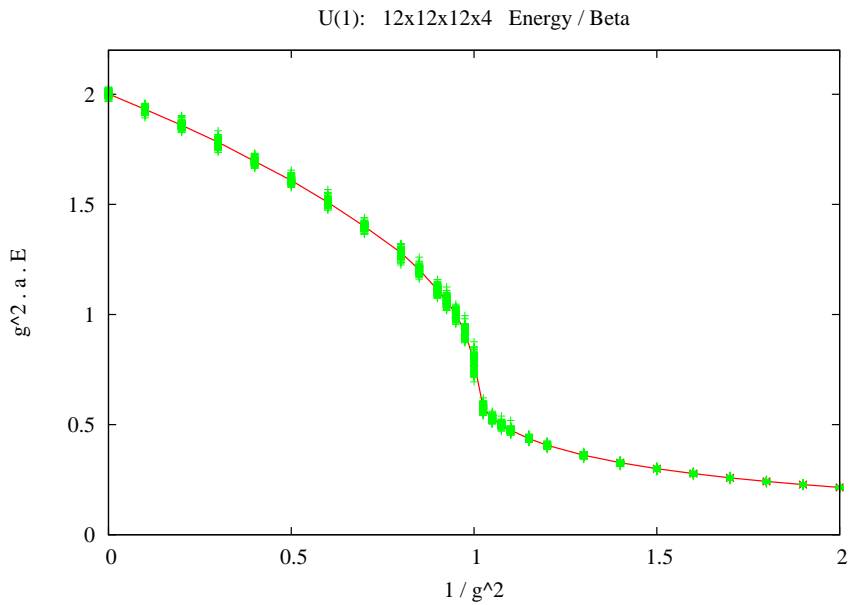


Figure 3.11 Transition of the plaquette energy as in Fig. 3.10.

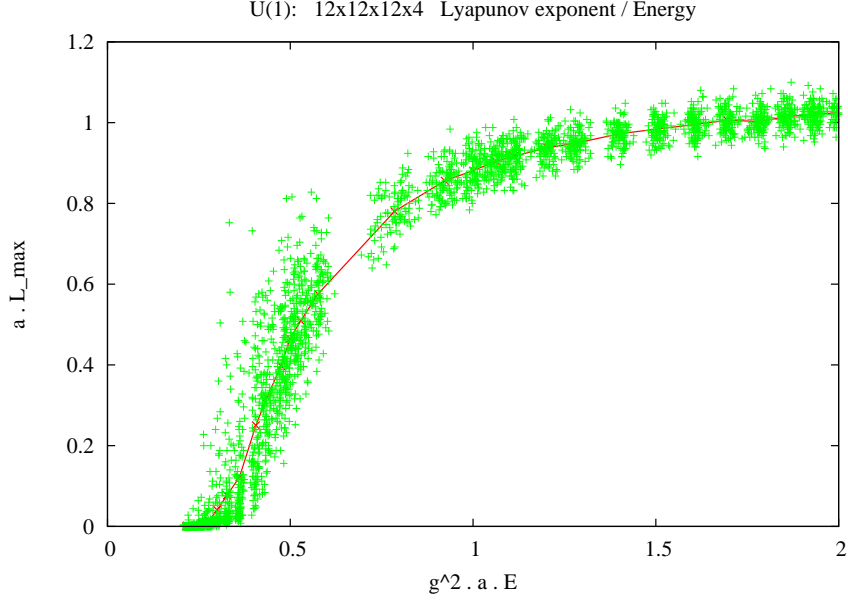


Figure 3.12 Scatter plots of Lyapunov exponents and plaquette energies for 100 $U(1)$ configurations.

and the energy [24, 32] is expected

$$L(a) \propto a^{k-1} E^k(a), \quad (3.1)$$

with the exponent k being crucial for the continuum limit of the classical field theory. A value of $k < 1$ leads to a divergent Lyapunov exponent, while $k > 1$ yields a vanishing L in the continuum. The case $k = 1$ is special leading to a finite non-zero Lyapunov exponent. Our analysis of the scaling relation (3.1) gives evidence, that the classical compact $U(1)$ lattice gauge theory has $k \approx 2$ and with $L(a) \rightarrow 0$ a regular continuum theory. The non-Abelian $SU(2)$ lattice gauge theory signals $k \approx 1$ and stays chaotic approaching the continuum.

Summarizing, we investigated the classical chaotic dynamics of $U(1)$ and $SU(2)$ lattice gauge field configurations prepared by quantum Monte Carlo simulation. The maximal Lyapunov exponent shows a pronounced transition as a function of the coupling strength. Both for QED and QCD we find that configurations in the strong coupling phase are substantially more chaotic than in the weak coupling regime. The results demonstrate that chaos is present when particles are confined, but it persists partly also into the Coulomb and quark-gluon-plasma phase. Already on the finite volume of the 12^3 lattice the first order of the $U(1)$ transition and the second order of the $SU(2)$ transition become visible.

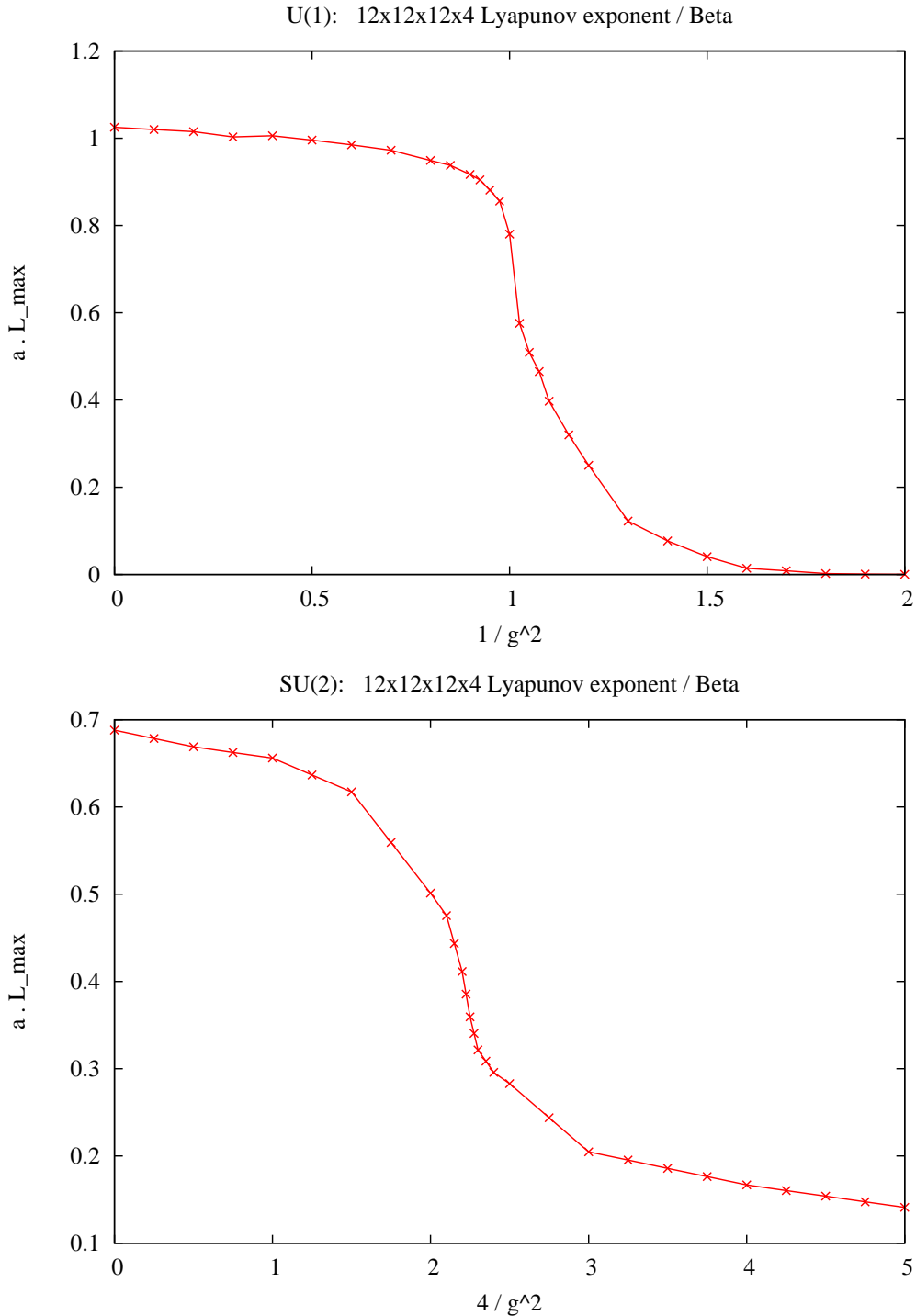


Figure 3.13 Comparison of the average maximal Lyapunov exponent in $U(1)$ gauge theory with $\beta = 1/g^2$ (top) and in $SU(2)$ gauge theory with $\beta = 4/g^2$ (bottom) when crossing from the strong to the weak coupling phase.

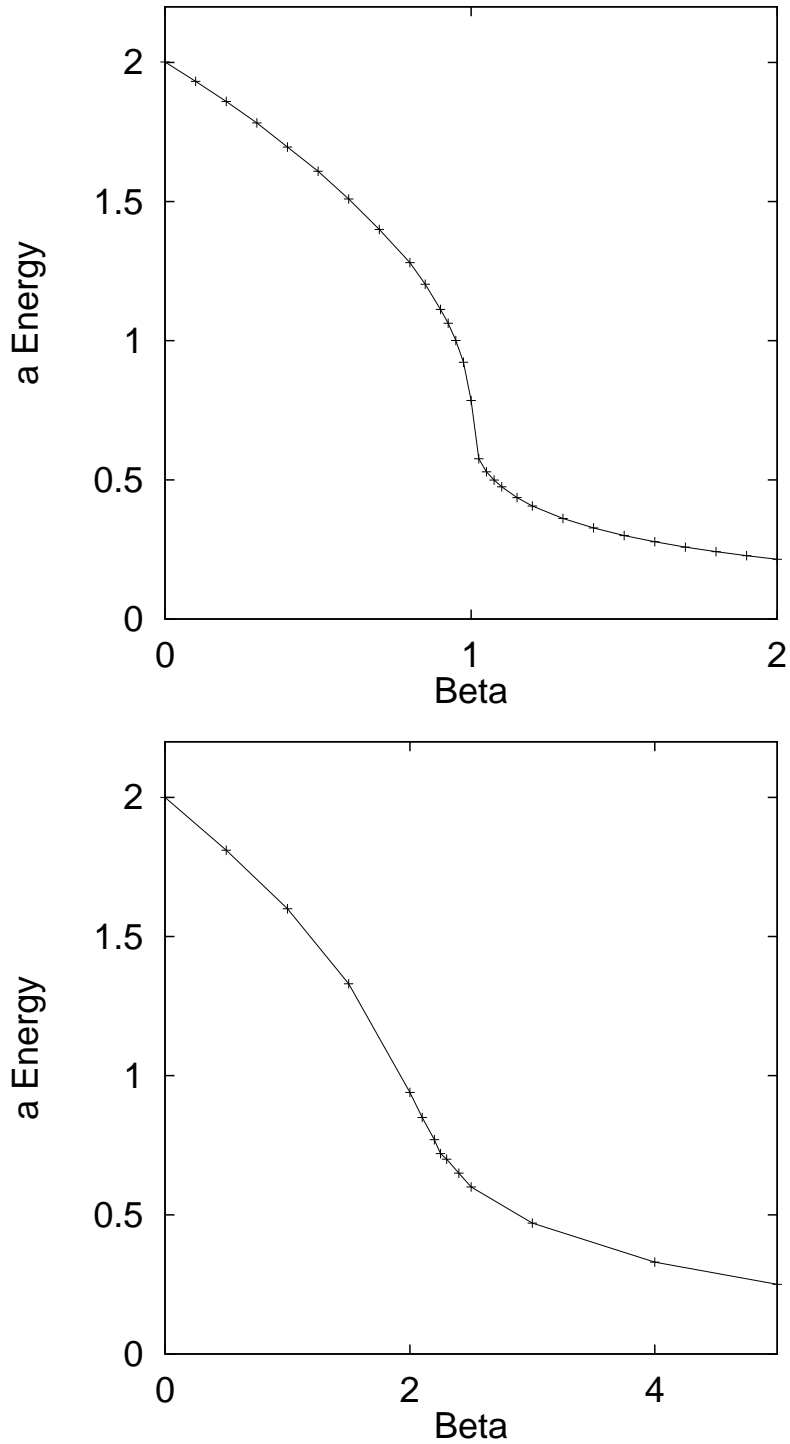


Figure 3.14 Comparison of the average plaquette energy as in Fig. 3.13

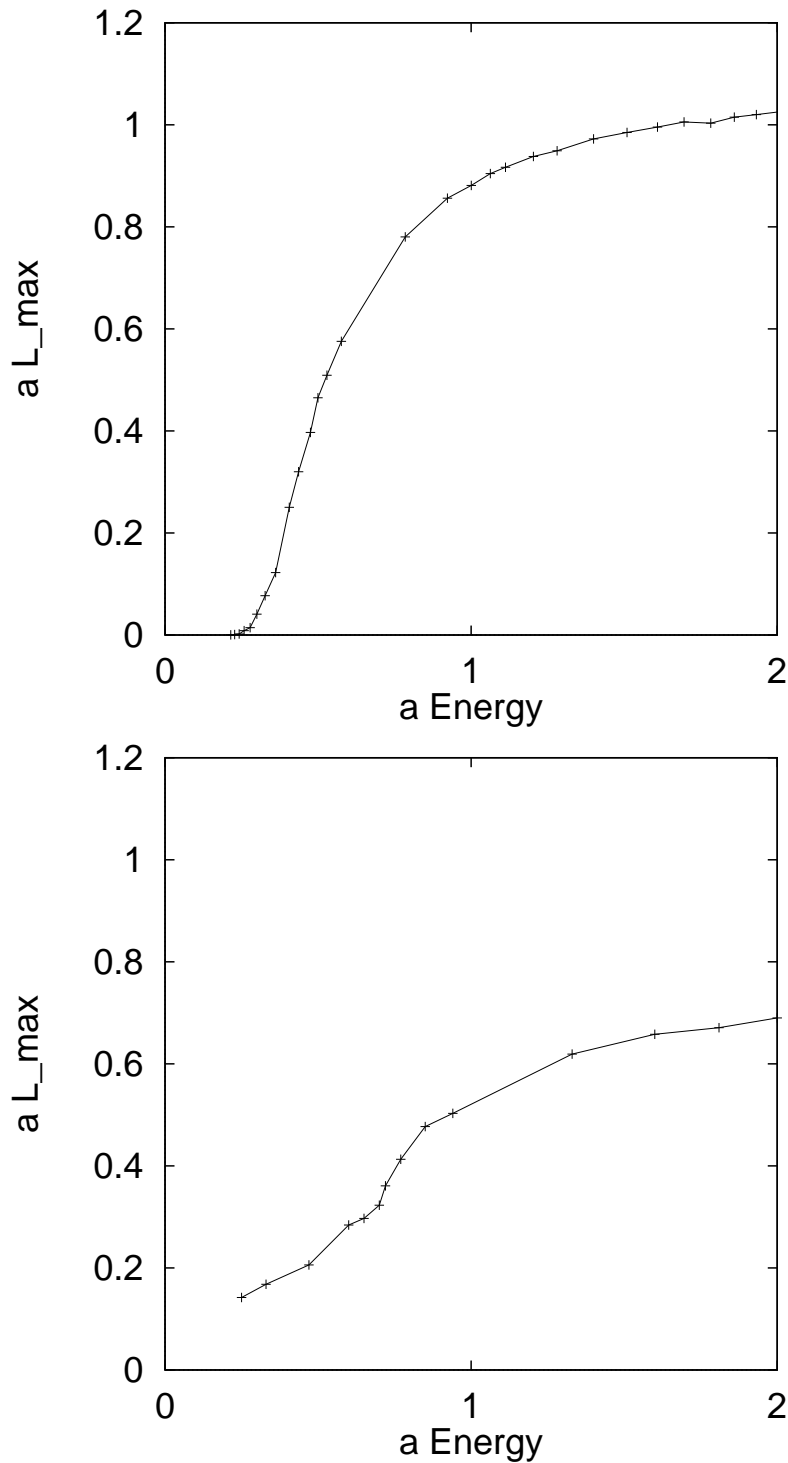


Figure 3.15 Comparison of average maximal Lyapunov exponents as a function of the scaled average energy per plaquette ag^2E . The $U(1)$ theory (top) shows an approximately quadratic behavior in the weak coupling regime whereas the $SU(2)$ theory (bottom) is approximately linear.

Turning to the preparation of the audio files, we multiplied the raw data by a factor of 1000 and added the standard pitch of 440 Hz. In Fig. 3.16 we depict the frequencies of the Lyapunov exponent in $U(1)$ gauge theory and in $SU(2)$ gauge theory from the confinement to the deconfinement phase. Listening to the corresponding sound files of $U(1)$ [web/cdrom] and of $SU(2)$ [web/cdrom] one can hear that the melody is changing clearly to lower tones. Both Lyapunov exponents behave similarly. Unfortunately, it is difficult to hear the difference between the 1st order of the $U(1)$ transition and the 2nd order of the $SU(2)$ transition. Those sound files can also be downloaded from the SonEnvir server [29].

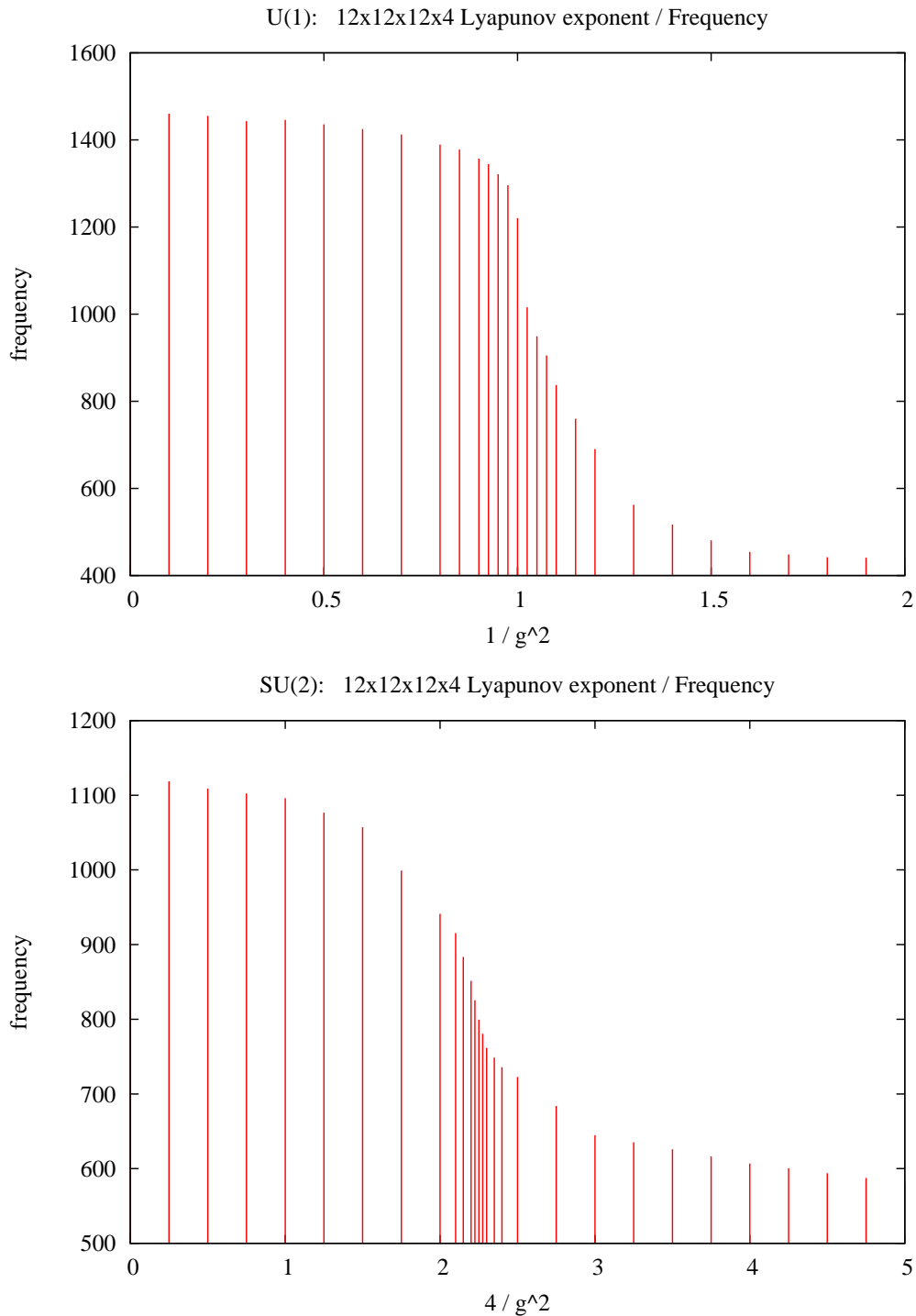


Figure 3.16 Comparison of the audible frequencies of the Lyapunov exponent in $U(1)$ gauge theory (top) and in $SU(2)$ gauge theory (bottom) when crossing from the strong to the weak coupling phase.

3.5 Physical Observables across Phase Transitions in Polymers

Monte Carlo simulations can be used not only for lattice QCD but have been designed generally for thermodynamic systems and their phase transitions. In this demonstration of sonification, we rely on a detailed study of the solubility-temperature phase diagram of a polymer in a cavity with an attractive substrate [33]. The Leipzig group identified the thermodynamic phases (Fig. 3.17) of adsorbed compact and expanded (AC, AE) and desorbed (DC, DE) conformations as well as the previously not yet clearly confirmed phase of adsorbed globules (AG). Although the polymer in the study possessed only $N = 179$ monomers, these (pseudo)phases are expected to be stable also in the thermodynamic limit $N \rightarrow \infty$. Other noticeable phase transitions in the compact-globular adsorbed regime (AC1-AC2d, AC1-AGe) are the energetic layering transitions from film-like surface-layer to double-layer conformations which are also believed to survive the thermodynamic limit. In addition, further subphases of higher-order layers were found in low-temperature regions and bad solvent (AC2a_{1,2}, AC2b, and AC2c). The most compact three-dimensional conformation found is cubelike and forms five layers (in subphase AC2a₁).

The (pseudo)phase diagram Fig. 3.17 is based on the profile of the specific heat C_V as a function of temperature T and reciprocal solubility s . Although this profile allows for the identification of phases and their boundaries it tells little about the conformational transitions between the phases. For this purpose they considered expectation values and fluctuations for the numbers of monomer-surface contacts, n_s , and intrinsic monomer-monomer contacts, n_m , separately, see Fig. 3.18. These contact numbers turned out to be sufficient to describe the macrostate of the system and therefore are useful to describe the conformations dominating the different phases [33].

We thank the Leipzig group for their data prior to publication to perform a sonification demonstration at the CompPhys05 workshop [34]. Listening to the result for the specific heat of the [polymers](#) [web/cdrom] along the T axis for $s = 1$ we experience the spike and the shoulder from the probably first-order transitions around $T \approx 0.34$ and $T \approx 2.44$, respectively. The SonEnvir project-group in Graz has also written a sonification tool for moving around the polymer landscape so that one can hear the polymer structure in the vicinity of the current position. Sample files are stored on the SonEnvir server [29].

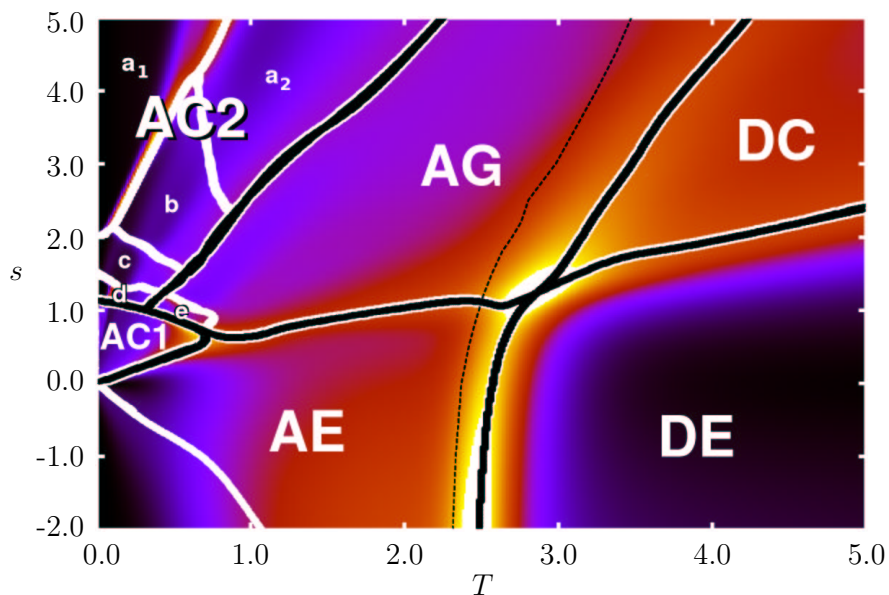


Figure 3.17 Solubility-temperature pseudophase diagram of a 179-mer simulated by the Leipzig group. The color codes the specific heat as a function of reciprocal solubility s and temperature T .

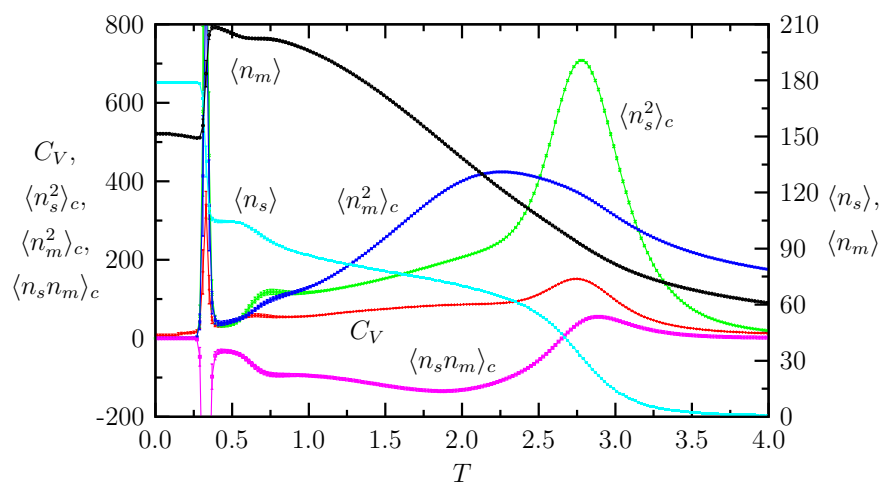


Figure 3.18 Expectation values, self- and cross-correlations of the contact numbers n_s and n_m as functions of the temperature T in comparison with the specific heat C_V for a 179-mer in solvent with $s = 1$. The specific heat from these results of the Leipzig group is taken for sonification.

Summary and Conclusion

This diploma thesis represents an attempt to learn about sonification in physics. The main goal was the application of auditory display to data from physical observables across phase transitions. The studies range from quantum chromodynamics to polymers. Central emphasis was on the phase transition of QCD from the confinement of quarks to the plasma of quarks and gluons. The physical observable was the eigenvalue spectrum of the Dirac operator of a quark in QCD. In two analyses of the lowest eigenvalues, keeping the gluonic coupling β fixed and letting β run, respectively, one could hear the restoration of chiral symmetry when increasing the coupling to the quark-gluon plasma-phase. Subsequently, the disorder parameter for magnetic monopoles was considered. One could hear the spike at the phase transition to the quark-gluon plasma where the monopoles vanish.

The next study was devoted to the leading Lyapunov exponents of $U(1)$ and $SU(2)$ classical gauge field configurations on the lattice. Although the breakdown of the Lyapunov exponent at the phase transition was clearly audible, it is difficult to distinguish between the first and second order of the transitions.

The last analysis dealt with Monte Carlo simulations of polymers. They exhibit a rich phase structure. Sonification rendered two transitions of presumably first order with different characteristics due to finite volume effects.

In the above first trials of sonification, the structures one could recognize from the sound files are similar to those from graphical visualization. In this regard,

sonification as applied here can be seen as an additional tool of data representation. Of course, it could be possible to find more refined means of auditory display in order to make further qualities apparent in some given data sets. Sonification offers the chance to detect structures in the data sets that have been hidden to the methods applied so far. Data analysis through sonification might especially be useful for displaying results depending on multiple parameters and/or belonging to higher space-time dimensions. In the context of lattice QCD it could be possible to demonstrate the topological content of certain gauge field configurations.

Concerning the sonification process only until one understands more about the human perception of sonification, the field will remain in trial-and-error state. The professional sonification tool we used, SuperCollider, is very powerful but difficult to work with. On one hand it requires some knowledge of a musician, on the other hand the program language is rather complex. It would be desirable to have a user interface with a limited instruction set for sonification similar to existing graphics packages. The development of such a sonification package is one of the aims of the SonEnvir project.

A

SuperCollider Functions

A.1 Short Introduction into the Function Syntax

SuperCollider has built-in functions for various kinds of sound sources (oscillators, noise generators, sounds file readers, live inputs), time functions (envelopes, controls), sound processors (filters, delay lines), and output (to write sound samples to the digital-to-analog convertor or to a file) [35].

“Synth”, “SinOsc”, “LFNoise” are objects, “play” and “ar” are messages. “{SinOsc.ar(LFNoise0.ar(10, 400, 800), 0, 0.3)}” is a function (everything between { and }, separated by commas). In the code “LFNoise0.ar(10, 400, 800)” the “.ar” is the message, so “(10, 400, 800)” is a list of three arguments for the “ar” message. Both “ar” and “kr” messages generate graphs describing sounds, but “ar” uses sample rates appropriate for audio signals (audio rate) while “kr” uses lower sample rates, appropriate for control signals (control rate).

A.2 Functions Used in the Lyapunov Program

A.2.1 Impulse – Impulse Oscillator

Impulse.ar(freq, phase, mul, add)

Outputs non band limited single sample impulses.

freq - frequency in Hertz

phase - phase offset in cycles (0..1)

```
{ Impulse.ar(800, 0.0, 0.5, 0) }.play
```

modulate phase:

```
{ Impulse.ar(4, [0, MouseX.kr(0, 1)], 0.2) }.play;
```

A.2.2 Decay2 – Exponential Decay

Decay2.ar(in, attackTime, decayTime, mul, add)

Decay has a very sharp attack and can produce clicks. *Decay2* rounds off the attack by subtracting one *Decay* from another.

Decay2.ar(in, attackTime, decayTime) is equivalent to:
Decay.ar(in, decayTime) - Decay.ar(in, attackTime)

in - input signal

attackTime - 60 dB attack time in seconds

decayTime - 60 dB decay time in seconds

```
plot({ Decay2.ar(Impulse.ar(1), 0.001, 0.01) })
```

```
// used as an envelope
```

```
{ Decay2.ar(Impulse.ar(XLine.kr(1,50,20), 0.25), 0.01, 0.2,  
FSinOsc.ar(600)) }.play;
```

A.2.3 Osc – Interpolating Wavetable Oscillator

Osc.ar(table, freq, phase, mul, add)

Linear interpolating wave-table lookup oscillator with frequency and phase modulation inputs.

This oscillator requires a buffer to be filled with a wave-table format signal. This preprocesses the Signal into a form which can be used efficiently by the Oscillator. The buffer size must be a power of 2.

This can be archived by creating a Buffer object and sending it one of the “b_gen” messages (sine1, sine2, sine3) with the wave-table flag set to true.

This can also be archived by creating a Signal object and sending it the “asWavetable” message, saving it to disk, and having the server load it from there.

table - buffer index

freq - frequency in Hertz

phase - phase offset or modulator in radians

note about wavetables:

OscN requires the b_gen sine1 wavetable flag to be OFF.

Osc requires the b_gen sine1 wavetable flag to be ON.

```
( s = Server.local; b = Buffer.alloc(s, 512, 1);
b.sine1(1.0/[1,2,3,4,5,6], true, true, true);

SynthDef("help-Osc",{ arg out=0,bufnum=0;
  Out.ar(out,
    Osc.ar(bufnum, 200, 0, 0.5)
  )
}).play(s,[\out, 0, \bufnum, b.bufnum]); )

( s = Server.local; b = Buffer.alloc(s, 512, 1);
b.sine1(1.0/[1,2,3,4,5,6], true, true, true);

SynthDef("help-Osc",{ arg out=0,bufnum=0;
  Out.ar(out,
    Osc.ar(bufnum, XLine.kr(2000,200), 0, 0.5)// modulate freq
  )
}).play(s,[\out, 0, \bufnum, b.bufnum]); )
```

A.2.4 AmpComp – Basic Psychoacoustic Amplitude Compensation

superclass: UGen

implements the (optimized) formula: $\text{compensationFactor} = (\text{root} / \text{freq})^{**} \text{exp}$

Higher frequencies are normally perceived as louder, which AmpComp compensates.

**ar(freq, root, exp)*

**kr(freq, root, exp)*

**ir(freq, root, exp)*

freq - input frequency value. For $\text{freq} == \text{root}$, the output is 1.0.

root - root freq relative to which the curve is calculated (usually lowest freq), default value: C (60.midiCps)

exp - exponent: how steep the curve decreases for increasing freq (cf. plot function), default value 0.3333

see also [AmpCompA]

```
// compare a sine without compensation
{ SinOsc.ar(MouseX.kr(300, 15000, 1)) * 0.1 }.play;

// with one that uses amplitude compensation
( {
  var freq;
  freq = MouseX.kr(300, 15000, 1);
  SinOsc.ar(freq) * 0.1 * AmpComp.kr(freq, 300)
}.play; )

// different sounds cause quite different loudness perception,
// and the desired musical behavior can vary, so the exponent can be tuned:
( {
  var freq;
  freq = MouseX.kr(300, 15000, 1);
  Pulse.ar(freq) * 0.1 * AmpComp.kr(freq, 300, 1.3)
}.play; )

// the curves:
// exp = 0.3333
(200,210..10000).collect {|freq| (200/freq) ** 0.3333 }.plot;
```

A.2.5 Splay

**ar(inArray, spread, level, center, levelComp)*

**arFill(n, function, spread, level, center, levelComp)*

Splay spreads an array of channels across the stereo field.

Optional spread and center controls, and levelComp(ensation) (equal power).

```
x = { arg spread=1, level=0.2, center=0.0;
  Splay.ar(
    SinOsc.ar( { |i| LFNNoise2.kr( rrand(10, 20), 200, 400) } ! 10),
    spread,
    level,
    center
  );
}.play;

x.set(\spread, 1, \center, 0); // full stereo \\
x.set(\spread, 0.5, \center, 0); // less wide
x.set(\spread, 0, \center, 0); // mono center \\
x.set(\spread, 0.5, \center, 0.5); // spread from center to right
x.set(\spread, 0, \center, -1); // all left \\
x.set(\spread, 1, \center, 0); // full stereo

// with mouse control
x = { var src;
  src = SinOsc.ar( { |i| LFNNoise2.kr( rrand(10, 20), 200, i + 3 * 100) } ! 10);
  Splay.ar(src, MouseY.kr(1, 0), 0.5, MouseX.kr(-1, 1));
}.play;
```

B

Lyapunov Program

Here we document a code example of the Sonification of the Lyapunov Exponent in $U(1)$ and $SU(2)$ theory. We use the graphical audio-editor *audacity* for the transformation of the output file format to mp3.

B.1 Sonification Program Lyapunov.sc

```
// Sonification of the Lyapunov-exponent in U(1) and SU(2) ...
```

```
Sound representation :
```

```
The exact rendering of the data as sound can be tuned extensively.  
The data property of interest, the Lyapunov exponent is mapped to  
frequency, and the beta values can be spread out as melodies  
within a loop.
```

```
Here are the tuning parameter names and what they mean:
```

```
slope :           can be used to make higher excitation levels  
                  softer. 0 is all levels equally loud.
```

```
panSpread :       the melody can be panned across 2 channels,  
                  panSpread 1 is fully spread, 0 is all in  
                  one (center) position.
```

```
panCenter :       the center pos of all tones: -1 is all left,  
                  0 is center, 1 is right.
```

```
attack :          attack time of the individual sounds; short is a  
                  hard attack, long is soft. must be greater than
```

```

        ringtime.

ringtime : how long each tone rings until it loses 99.9% energy.

bgLevel : raises the minimum volume of each value so that
          one hears all tones together as a background
          sound.

attSpread : how far apart in time within the loop the tones
           are spaced. 0 is all attacks together, 1 is spread
           over the full time of the loop.

attDelay   : 0 means first value plays instantly, can be
             delayed to hear background tones before indiv.
             tones.

loopTime   : how long one repetition of the melody should last.

The Tdef (Task) steps through both gauge fields u(1) and su(2).

( var pathname, recfilename;

q = q ? (); p = ProxySpace.push;

    // read the data from u(1) and su(2) models
    // change path to data file here

pathname = "D:/Daten/Sonification/";

recfilename = ["lyapunov_input_u1.txt", "lyapunov_input_su2.txt"];

q.rawData = TabFileReader.read(pathname ++ recfilename.[0], true,
true);

q.rawData = q.rawData ++ TabFileReader.read(pathname ++
recfilename.[1], true, true);

q.names = q.rawData.first; q.dataOnly = q.rawData.select { |line|
line.first.first.isDecDigit };

q.dataOnly = q.dataOnly.collect { |line, i|

    // 29 values of the input-file u(1) and 29 values of the
    // input-file su(2)

[ (i div: 29), i % 29 ] ++ line.collect(_.asFloat);

}.printAll;

q.data = Data(\lyapunov, [\gaugefield, \index, \beta, \lyapexp,
\freq ], q.dataOnly.flop);

    // make a sine wavetable for the osc.
b = Buffer.alloc(s, 1024, 1, bufnum: 440); b.sine1([1]);

)

    // Sound function
( // dynamic/spreadout settings

```

```

~lyapexp = { arg spread=1,
  slope=0, panSpread=1, panCenter=0.0,
  attack=0.01, ringtime=2.0, bgLevel=0.0,
  attDelay=0.15, attSpread=0.85, looptime=10;

  var freqs, amps, size, trigs;

  // sets the frequency to 440 Hz
  freqs = Control.names([\freqs]).kr(((1 .. 29) + 440));
  size = freqs.size;

  freqs = freqs.lag(0.2);
  trigs = Impulse.kr(
    looptime.reciprocal,
    (0.. freqs.size-1).reverse / size * attSpread
    + (attSpread.min(0).abs) + attDelay
  ) * Line.kr(0, 1, 0.1).squared;

  amps = Decay2.kr(
    trigs,
    attack,
    ringtime * (60.midicps / freqs ** 0.25)
  ).max(bgLevel);

  amps = amps * (0.5 ** ((0..freqs.size - 1) * slope)) * 4;

  // for stereo sound
  Splay.ar(Osc.ar(440, freqs, 0, AmpComp.kr(freqs.max(100),
    exp: 0.4) * amps),
    spread: panSpread,
    center: panCenter
  );
}; ~lyapexp.play(vol: 1.0); )

  // allocate the input frequency of u(1)
~lyapexp.setn(\freqs, q.data[4].clump(29).[0]);
~lyapexp.end;
~lyapexp.play;

  // allocate the input frequency of su(2)
~lyapexp.setn(\freqs, q.data[4].clump(29).[1]);
~lyapexp.end;

( // record files Task {
  var pathname, recfilename;
  pathname = "D:/Daten/Sonification/";
  recfilename = ["Lyapunovul", "Lyapunovsu2"];

  s.recSampleFormat_("int16").recHeaderFormat_("WAV");
  ~lyapexp.end;
  0.5.wait;

  [0, 1].do { |i|
    var freqs;
    // freq values
    freqs = q.data[4].clump(29).[i];
    ~lyapexp.setn(\freqs, freqs, \attDelay, 0.02);
    s.prepareForRecord(pathname ++ recfilename.[i] ++ ".wav");
    0.5.wait;
    s.record;
    0.1.wait;
    ~lyapexp.play(fadeTime: 0.01);
  }
);

```

```
        11.3.wait;  
        ~lyapexp.end(0.1);  
        0.5.wait;  
        s.stopRecording;  
    };  
    "done.".postln;  
}.play; )
```

B.2 Input File lyapunov_input_u1.txt

```

For Beta = 0.0 - 2.0 - U(1)
beta      Lyapunov-exponent    frequency

0.0000    1.02514851485148      1465.148515
0.1000    1.01988118811881     1459.881188
0.2000    1.01504950495049     1455.049505
0.3000    1.00312871287128     1443.128713
0.4000    1.00570297029702     1445.70297
0.5000    0.99568316831683     1435.683168
0.6000    0.98487128712871     1424.871287
0.7000    0.97243564356436     1412.435644
0.8000    0.94902970297030     1389.029703
0.8500    0.93794059405941     1377.940594
0.9000    0.91691089108911     1356.910891
0.9250    0.90443564356436     1344.435644
0.9500    0.88122772277228     1321.227723
0.9750    0.85607920792079     1296.079208
1.0000    0.78023762376238     1220.237624
1.0250    0.57564356435644     1015.643564
1.0500    0.50899009900990     948.990099
1.0750    0.46510891089109     905.1089109
1.1000    0.39714851485149     837.1485149
1.1500    0.31992079207921     759.9207921
1.2000    0.25041584158416     690.4158416
1.3000    0.12245544554455     562.4554455
1.4000    0.07699009900990     516.990099
1.5000    0.04099009900990     480.990099
1.6000    0.01429702970297     454.2970297
1.7000    0.00859405940594     448.5940594
1.8000    0.00201980198020     442.019802
1.9000    0.00087128712871     440.8712871
2.0000    0.00031683168317     440.3168317

```

B.3 Input File lyapunov_input_su2.txt

```

For Beta = 0.0 - 5.0 - SU(2)
beta      Lyapunov-exponent      frequency
0.0000    0.68800004025765          1128.000040
0.2500    0.67845763553409          1118.457636
0.5000    0.66891523081052          1108.915231
0.7500    0.66245575684380          1102.455757
1.0000    0.65599628287708          1095.996283
1.2500    0.63661786097692          1076.617861
1.5000    0.61723943907676          1057.239439
1.7500    0.55925097960279          999.250980
2.0000    0.50126252012882          941.262520
2.1005    0.47542462426194          915.424624
2.1501    0.44342086688137          883.420867
2.1998    0.41141710950081          851.417110
2.2249    0.38543240740741          825.432407
2.2500    0.35944770531401          799.447705
2.2751    0.34050970209340          780.509702
2.3002    0.32157169887279          761.571699
2.3499    0.30865275093935          748.652751
2.3995    0.29573380300591          735.733803
2.5000    0.28281485507246          722.814855
2.7500    0.24376439881911          683.764399
3.0000    0.20471394256575          644.713943
3.2500    0.19524494095545          635.244941
3.5000    0.18577593934514          625.775939
3.7500    0.17630693773484          616.306938
4.0000    0.16683793612453          606.837936
4.2500    0.16037846215781          600.378462
4.5000    0.15391898819109          593.918988
4.7500    0.14745951422437          587.459514
5.0000    0.14100004025765          581.000040

```

Acknowledgments

First of all I want to thank my advisor Harald Markum, who raised the idea to this diploma thesis, for his helpful support during all the work. I am also very grateful to Alberto de Campo from the University for Music and Dramatic Arts in Graz, Katharina Vogt and Willibald Plessas from the University of Graz for helping me with the sonification programs, developing interesting ideas and bringing in their experience in this new research area. I am indebted to Rainer Pullirsch for his prior work producing the eigenvalue spectra of the Dirac operator and Tamás S. Biró from the Research Institute for Particle and Nuclear Physics, Budapest who supported me writing the program for the Lyapunov exponents in QED and enabled me to participate at the QCD conference in Montpellier, France.

A very special thank belongs to my family and my friends Christa Köstner, Gerhard Köstner, Edith Lunacek, Rudolf Hörmann, Gerald Hörmann, Michael Schlögl, Sylvia Weninger and Johannes Köck. They especially supported me all the time, helped me to keep up and had understanding for my limited time for them during my studies.

Bibliography

- [1] [http://www.techfak.uni-bielefeld.de/ags/ni/projects/datamining/datason/datason_e.html]
- [2] [<http://spdf.gsfc.nasa.gov/research/sonification/documents/Chapter5.pdf>]
- [3] [<http://www.icad.org/>]
- [4] [<http://www.icad.org/websiteV2.0/References/nsf.html>]
- [5] [<http://www.sonenvir.at/>]
- [6] [<http://en.wikipedia.org/wiki/Sonification>]
- [7] A. de Campo, C. Frauenberger, R. Höldrich, T. Melde, W. Plessas, B. Sengl, *Sonification of quantum spectra*, in Proceedings of ICAD 05 - Eleventh Meeting of the International Conference on Auditory Display, Limerick, Ireland, July 6-9, 2005 [<http://www.idc.ul.ie/icad2005/downloads/f67.pdf>].
- [8] K. Rabitsch, *Hadron-Hadron Potentials from Lattice Quantum Chromodynamics*, Doctoral Thesis, Vienna University of Technology (1997).
- [9] R. Pullirsch, *Quantum Chaos in the Dirac Spectrum of Lattice Quantum Chromodynamics*, Diploma Thesis, Vienna University of Technology (1998).
- [10] P. Becher, M. Böhm, H. Joos, *Eichtheorien der starken und elektroschwachen Wechselwirkung*, Teubner (Stuttgart 1983).
- [11] R.P. Feynman, A.R. Hibbs, *Quantum Mechanics and Path Integrals*, McGraw-Hill (New York 1965).
- [12] K.G. Wilson, *Confinement of quarks*, Phys. Rev. D10 (1974) 2445.

- [13] A. Hasenfratz, P. Hasenfratz, *Lattice gauge theories*, Ann. Rev. Nucl. Part. Sci 35 (1985) 559.
- [14] L.H. Karsten, J. Smit, *Lattice fermions: Species doubling, chiral invariance, and the triangle anomaly*, Nucl. Phys. B183 (1981) 103.
- [15] H.B. Nielsen, M. Ninomiya, *Absence of neutrinos on a lattice*, Nucl. Phys. B185 (1981) 20.
- [16] J. Kogut, L. Susskind, *Hamiltonian formulation of Wilson's lattice gauge theories*, Phys. Rev. D11 (1975) 395.
- [17] L. Susskind, *Lattice fermions*, Phys. Rev. D16 (1977) 3031.
- [18] H. Neuberger, *Lattice chirality*, LATTICE98, Nucl. Phys. Proc. Suppl. 73 (1999) 697-699 [hep-lat/9807009].
- [19] F. Niedermayer, *Exact chiral symmetry, topological charge and related topics*, LATTICE98, Nucl. Phys. Proc. Suppl. 73 (1999) 105-119 [hep-lat/9810026].
- [20] A. Di Giacomo, B. Lucini, L. Montesi, G. Paffuti, *Colour confinement and dual superconductivity of the vacuum - I*, Phys. Rev. D61 (2000) 034503 [hep-lat/9906024].
- [21] A. Di Giacomo, B. Lucini, L. Montesi, G. Paffuti, *Colour confinement and dual superconductivity of the vacuum - II*, Phys. Rev. D61 (2000) 034504 [hep-lat/9906025].
- [22] W. Sakuler, *Topologische Ladungsdichte um statische Quarks in der Gitter-Quantenchromodynamik*, Doctoral Thesis, Vienna University of Technology (1994).
- [23] T.S. Biro, N. Hörmann, H. Markum, R. Pullirsch, *Chaos analyses in both phases of QED and QCD*, in Proceedings of QCD'99, July 07-13, 1999, Montpellier, France, Nucl. Phys. Proc. Suppl. 86 (2000) 403-407 [hep-ph/9909309].
- [24] T.S. Biró, S.G. Matinyan, B. Müller, *Chaos and Gauge Field Theory*, World Scientific (Singapore 1995).
- [25] T.S. Biró, *Conserving algorithms for real-time nonabelian lattice gauge theories*, Int. J. Mod. Phys. C (Computational Physics) 6 (1995) 327-344.

- [26] T.S. Biró, M. Feurstein, H. Markum, *Chaotic behavior of confining lattice gauge field configurations*, APH Heavy Ion Physics 7 (1998) 235 [hep-lat/9711002].
- [27] R. Pullirsch, K. Rabitsch, T. Wettig, H. Markum, *Evidence for quantum chaos in the plasma phase of QCD*, Phys. Lett. B427 (1998) 119 [hep-ph/9803285].
- [28] A. de Campo, N. Hörmann, H. Markum, W. Plessas, B. Sengl, *Sonification of lattice data: The spectrum of the Dirac operator across the deconfinement transition*, in Proceedings of Lattice 2005 - XXIII International Symposium on Lattice Field Theory, Dublin, Ireland, July 25-30, 2005, PoS(LAT2005)152 [<http://www.sonenvir.at/downloads/LatticeQCD/SonifLatticeData.pdf>].
- [29] [<http://www.sonenvir.at/downloads/LatticeQCD>]
- [30] A. de Campo, N. Hörmann, H. Markum, W. Plessas, B. Sengl, *Sonification of lattice observables across phase transitions*, in Proceedings of International Workshop on Extreme QCD, August 2-5, 2005, University of Wales, Swansea, in print [<http://www.sonenvir.at/downloads/LatticeQCD/SonifLatticeSwansea.pdf>].
- [31] A. de Campo, N. Hörmann, H. Markum, W. Plessas, K. Vogt, *Sonification of lattice data: Dirac spectrum and monopole condensation along the deconfinement transition*, in Proceedings of Miniconference in honor of Adriano Di Giacomo on the Sense of Beauty in Physics, January 26-27, 2006, Pisa, Italy, in print [http://www.sonenvir.at/downloads/LatticeQCD/DGfest_markum.pdf].
- [32] L. Casetti, R. Gatto, M. Pettini, *Geometric approach to chaos in the classical dynamics of Abelian lattice gauge theory*, J. Phys. A32 (1999) 3055 [chao-dyn/9810033];
H.B. Nielsen, H.H. Rugh, S.E. Rugh, *Chaos, scaling and existence of a continuum limit in classical non-Abelian lattice gauge theory*, ICHEP96, 1603 [hep-th/9611128];
B. Müller, *Study of chaos and scaling in classical SU(2) gauge theory* [chao-dyn/9607001];
H.B. Nielsen, H.H. Rugh, S.E. Rugh, *Chaos and scaling in classical non-Abelian gauge fields* [chao-dyn/9605013].
- [33] M. Bachmann, W. Janke, *Substrate adhesion of a nongrafted polymer in a cavity*, Phys. Rev. E73 (2006) 041802.

[34] [<http://www.physik.uni-leipzig.de/~janke/CompPhys05/>]

[35] [<ftp://ftp.create.ucsb.edu/pub/SuperCollider/Book/Book.pdf>]